1992

Mechanical circulatory assist : a device for direct ventricular compression

John J. Pacella
Lehigh University

AUTHOR:

Pacella, John J.

TITLE:

Mechanical Circulatory Assist: A Device for Direct Ventricular Compression

DATE: October 11, 1992

Mechanical Circulatory Assist:
A Device for Direct Ventricular Compression

by

John J. Pacella

A Thesis

Presented to the Graduate Committee

of Lehigh University

in Candidacy for the Degree of

Master of Science

in Mechanical Engineering

Lehigh University

September 1992

This thesis is accepted in partial fulfillment of the requirements for the degree of Master of Science.

Sept. 29, 1992

(date)

Professor Eric P. Salathe

Professor Robert P. Wei

Chairman of the Department

Acknowledgements

The author expresses sincere gratitude to Dr. Eric Salathe for his guidance and genuine interest in this formidable undertaking. Special thanks are in order to Susan Fontana, William Lackey, Mr. and Mrs. John N. Pacella, Mark S. Schnabel, and Mr. and Mrs. Ronald L. Fontana for their support.

Furthermore, thanks to Dr. Michael Sinclair, David Rice, and the staff at Lehigh Valley Hospital for their assistance during the primary animal experiment. Finally, thanks to Dr. Goldstein, Dennis Trumble, Dr. Cmolik, Dr. Park, Dr. Anderson, and Tom Loebig at Allegheny General Hospital for their patience and advice.

Table of Contents

List of Figures

Abstract

A mechanical biventricular assist device for automatic cardiac massage has been developed through a highly refined production process. It has been tested *in vitro* and *in vivo* and its efficacy as a circulatory assist device is being determined.

The device consists of a distensible external polyurethane shell that internally supports two inflatable bladders. Inflation of the two bladders results in compression of the native ventricles and production of systolic pressure. Since the device does not contact blood, it can be applied rapidly for immediate circulatory support.

An experimental method for quantifying the *in vitro* hemodynamic effects of the device utilizing state-of-the-art myocardial deformation tracking techniques has been developed. Through the use of shell theory, the mechanical interaction between the myocardial wall and the device bladder has been analyzed.

Bench and animal experiments have revealed that this device deserves further consideration as an effective circulatory assist tool.

1 Introduction

This project involved the design, development, and testing of a mechanical biventricular assist device (MBAD). The project was conceived in 1987 by Dr. Eric Salathe. Past research has led to the formulation of a potential production scheme for the MBAD.

The objective of the present project was to renovate the production method, improve the design of the MBAD, and perform thorough *in vitro* and *in vivo* testing. In addition to the accomplishment of this objective, a research protocol for *in vivo* quantification of device performance has been developed. Also, a mechanical analysis relating physiological interaction with the device which utilizes shell theory has been performed.

Currently, the device is prepared for more extensive *in vivo* and *in vitro* testing and evaluation; measurement of assisted and unassisted cardiac deformation, cardiac output, and pulmonary and systemic pressures will provide additional information regarding device performance.

2 Background Information

An understanding of the function of the human heart is critical to the development of an effective circulatory assist device. These types of devices can be used to alleviate the multiple forms of cardiac dysfunction. As a result, the field of bioengineering has explored the varied ways in which assist can be applied. Currently, there are many forms of circulatory assist. In particular, direct mechanical ventricular assistance is a novel method for the application of cardiac massage. Through his findings, G.L. Anstadt [1] provided the basis for the development of a device for direct ventricular compression.

2.1 Function of the Heart

2.11 Normal Cycle

The cardiac cycle of the four chambered human heart consists of two phases, systole and diastole. During systole, the left and right ventricles contract and propel blood into the systemic and pulmonary circulation. In diastole, the heart refills with blood in preparation for the next contraction. Typically, the heart spends 70% of its time in diastole during a cardiac cycle.

There are four valves that operate in the heart to maintain normal pressure and flow. The two atrio-ventricular valves are located between the atria and the ventricles; these are one-way valves that allow the pressure in the ventricles to increase without regurgitation of blood into the atria. The two semilunar valves are one-way valves that are located in the pulmonary artery and aorta; these prevent retrograde flow of blood into the ventricles (Figure 1, 2).

The heart receives its supply of oxygen and nutrients through its own coronary perfusion. The right and left main coronary arteries supply oxygen rich blood to the cardiac tissue primarily during diastole, when the heart muscle is relaxed. They receive their supply through the coronary os, the coronary artery openings in the aortic arch.

Electrical excitation of the heart is initiated in the sinoatrial node. Activation of this node causes atrial contraction. The electrical signal from this node arrives at the atrioventricular node about 1/10 of a second later. The signal at this node then causes ventricular contraction. The delay of 1/10 of a second allows enough time for blood flow between the atria and ventricles (Figure 3).

2.12 Cardiac Abnormalities

Heart disease is the leading cause of death in the United States, claiming almost 35,000 lives every year. In some cases, the severity of heart dysfunction warrants the need for transplant. Unfortunately, the limited availability of donor hearts forces patients who desperately need transplants to wait. As a bridge to transplant, assist devices and artificial hearts are being used to maintain circulation in the ailing patient until a donor heart becomes available.

In patients where heart dysfunction is not as severe, heart transplantation is not necessary and mechanical circulatory assistance can be provided. In these cases, the devices are meant to assist the heart by circulating blood throughout the body; this provides an opportunity for the heart to rest and eventually repair itself.

Presently, there are two indications when circulatory assist is needed. The first is cardiogenic shock that is unresponsive to medical treatment. In this case, a patient who has undergone open heart surgery is considered to have temporary ventricular dysfunction. Accordingly, an assist device is implanted on a temporary basis. Secondly, the need for circulatory assist occurs in patients who decompensate hemodynamically while awaiting a donor heart for transplant. In these cases, the ventricles are not expected to regain function. Overall, many of these disease states have been alleviated through the various forms of circulatory support.

2.2 Forms of Circulatory Assistance

Although mechanical circulatory assistance dates back to 1965, the advent of new technology has increased the overall successes in this area. In the past, circulatory assist was primarily administered to patients with postcardiotomy cardiogenic shock. However, the scope of patients has increased to include those with shock following acute myocardial infarction, as well as those who deteriorate before or after heart transplantation.

In all, there are a variety of types of circulatory assist pumps, including rotary pumps, roller pumps, sac-type pumps, and electrically driven pumps. The primary forms of circulatory assistance are rotary pumps and intra-aortic balloon pumps (IABP). Rotary pumps rely on a high speed impeller to drive blood, while the IABP utilizes compressed air to augment the cardiac cycle.

A common type of rotary pump is the centrifugal pump, which is typically used to provide left ventricular assist. This pump consists of a blood chamber with an inlet and outlet port. Generally, the inlet of the pump is inserted into the left atria or into the left ventricle through the mitral valve.

The outlet port is fastened to the descending aorta through an end-to-side anastomoses. An impeller located inside the blood chamber is coupled to a rotor and powered through a DC brushless motor. The impeller is usually rotated between 3000-5000 RPM.

Typically, the centrifugal pump is used for circulatory support either as an implant or extracorporeally. However, this device is best suited for short term application, as long term use often results in mechanical deterioration, fibrin deposition, hemolysis, and end-organ dysfunction.

Axial pumps are similar to centrifugal pumps in design except for their small size and slender shape. In order to compensate for size difference they must be operated at much higher speeds to move equivalent amounts of blood. These pumps are slender tubes that enclose a tiny impeller. In one particular application, they are inserted into the femoral artery and are guided into the left ventricle to provide assist. While in the left ventricle, the impeller is rotated at high speeds (25,000 in some cases) to effectively move blood into the systemic circulation. The major drawbacks associated with this type of pump are substantial hemolysis and excessive mechanical wear. Hemolysis occurs when the high speed impeller blades actually lyse red blood cells into fragments. High rotational speeds cause greater friction loss and eventual mechanical deterioration.

The IABP is another common method of assist. It is a plastic device that is usually positioned in the descending aorta via the femoral artery. The balloon itself is several inches in length, and it is inflated and deflated to provide systolic unloading and diastolic augmentation. It is controlled by the ECG signal or arterial pressure through a console. The balloon is inflated during diastole. This displaces a volume of blood equivalent to that of the

balloon, causing an increase in both arterial diastolic pressure and flow rate to the systemic circulation. This augments coronary perfusion, since the displaced blood between the balloon and the coronary os drains into the coronary arteries. At the end of diastole, the ECG triggers deflation, and the systolic pressure in the aorta (afterload) is lowered. This decreases the amount of cardiac energy that is required to eject a given stroke volume and diminishes the oxygen requirement of the myocardium.

Besides rotary pumps and intra-aortic balloon pumps, roller pumps, sac-type pumps, and electrically driven pumps are also available. However, the latest advancement in circulatory assist systems is pulsatile flow assist devices. One particular method of pulsatile flow assist is direct mechanical ventricular assistance.

2.3 Direct Mechanical Ventricular Assistance

Direct Mechanical Ventricular Assistance (DMVA) is an innovative method for the application of automatic cardiac massage first conceived by G.L. Anstadt [1]. It is accomplished through the use of a pneumatic biventricular assist device known as the Anstadt Cup. This device consists of a rigid, heart size, glass outer shell which is placed around the heart. The shell supports two inflatable bladders on its inner surface. Pneumatic pressure lines are attached to the bladders to allow inflation. The bladders are positioned on the shell in order to make contact with the ventricles. When the bladders are inflated, a compressive force acts on each of the ventricles, forcing blood out of the heart to the pulmonary artery and the aorta. In order to secure the cup to the heart, negative pressure is applied to the apex via a

tube fastened to the base of the shell. Filling and evacuation of the bladders is controlled through a timed circuit with solenoid valves.

In order to test the efficacy of DMVA, G.L. Anstadt performed a variety of animal studies in which it was used in the following scenarios:

- Circulatory Support Following Ventricular Fibrillation.
- Resuscitation Following Cardiac Arrest
- Circulatory Support Following Ischemia
- Circulatory Support Following Myocardial Infarction
- In vivo Organ Preservation
- Comparative Studies With Cardiopulmonary Bypass

These studies proved the usefulness of the Anstadt Cup as it underwent a series of intensive testing procedures under various modes of cardiac dysfunction.

Circulatory Support Following Ventricular Fibrillation

Several experiments by G.L. Anstadt revealed the effectiveness of DMVA as circulatory support following ventricular fibrillation, a non-linear contractile state of the left ventricle. In one particular experiment, DMVA was used to support a dog for 8 hours [3]. In later experiments [4], animals were sustained for 24-40 hrs with a 50% survival rate. In fact, infection was the cause of death for 8 out of 10 of the animals that did not survive. DMVA was also demonstrated to support circulation during 3 days of ventricular fibrillation (VF) with long term survival [5]. The hemodynamics produced by the device were found to be near normal.

Resuscitative Circulatory Support

DMVA was used for circulatory support following cardiac arrest in 1967 [6]. It was applied through a thoracotomy after a 5 minute ventricular fibrillation for 2.5-4 hours. 50% of the animals tested were found to achieve normal hemodynamics after the assist device was applied.

In other cases of cardiac arrest, myocardial infarction was induced through ligation of the left circumflex coronary artery [7]. DMVA was then applied for 5 hours and was found to supply normal hemodynamics to 95% of the animals. DMVA was also compared to open chest cardiac massage (OCCM) [8]. Circulatory arrest was induced for five minutes in dogs and either DMVA or OCCM was applied. OCCM incurred only 17% successful resuscitation, while DMVA produced 83%.

The standard therapy for cardiac arrest is closed chest cardiac massage (CCCM). However, in 1983 McCabe [9] compared CCCM to DMVA and found that DMVA increased circulatory hemodynamics three times that of CCCM. This same experiment was verified in 1984 by Bartlett [10] who found that DMVA produced flows 256-340% greater than CCCM.

DMVA was also found to significantly increase myocardial perfusion. This was verified by Brown [11] who induced VF in swine and then applied CCCM to some while applying DMVA to others. Brown determined that DMVA not only provided a cardiac output of seven times that of CCCM but also provided the endocardium with forty times the perfusion.

Circulatory Support Following Ischemia

In order to study the effect of DMVA after myocardial ischemia, the left anterior descending coronary artery of several dogs were occluded by Anstadt

[12]. After 90 minutes of occlusion, the ligature was removed and reperfusion was allowed. The dogs were then randomized into two groups. The first group received standard drug therapy for circulatory stabilization. Ventricular fibrillation was induced in the second group, and DMVA was applied. No evidence of myocardial necrosis was found in the dogs that underwent DMVA. This demonstrates that DMVA can actually salvage areas of ischemia and prevent infarction.

Circulatory support following myocardial infarction

DMVA was applied in several canine studies in order to treat myocardial infarction [13]. In most cases, the left circumflex coronary artery (LCA) was occluded for 5 hours to induce myocardial infarction, and DMVA was applied to some of the animals. The application of DMVA resulted in higher canine survival rates in all instances. For example, only 4 dogs that received standard medical therapy for treatment of myocardial infarction survived for one week. However, 15 dogs survived for one week following myocardial infarction (MI) with application of DMVA. This same trend was seen over 24 hours. In this case, a study in 1969 [13] revealed that 4 dogs survived for 24 hours receiving standard medical therapy, whereas 12 survived with DMVA.

***In vivo* organ preservation**

When organs are harvested for transplant, mechanical circulatory assist devices are often used to maintain organ perfusion. Several studies using DMVA for this purpose have been done. The first of these involved the use of DMVA to preserve organs after cardiac arrest [6]. Dogs were

arrested and DMVA was applied. Their kidneys were then transplanted or tested histologically and were found to be healthy for transplantation. In another case, a 32 year female who deceased following a one hour cardiac arrest was administered DMVA to maintain kidney perfusion [14]. The perfused kidney was transplanted, and the recipient was discharged shortly thereafter. At Johns Hopkins, DMVA was used for organ perfusion after much longer periods of cardiac arrest [15]. For example, animals were arrested for 15-20 minutes and were then provided with either DMVA or OCCM. The animals that received DMVA were found to have much healthier renal function than the animals who received OCCM. In deceased humans, DMVA was applied for 1-5 hours following cardiac arrest to assess renal perfusion. In 4 patients, adequate renal perfusion was immediately attained and remained constant until device removal. DMVA was also found to provide adequate organ perfusion to the liver and lungs in other studies by Veith [16].

Comparative Studies with Cardiopulmonary Bypass

Many studies by Anstadt have compared DMVA to cardiopulmonary bypass (CPB). One particular study viewed DMVA and CPB support following ventricular fibrillation [17]. In this case, ischemia was not present using either method. Studies have also revealed that DMVA can be applied more quickly and provides more adequate renal cortex perfusion and myocardial perfusion [17]. Finally, Anstadt [18] has shown that DMVA supplies higher myocardial ATP levels and more ischemic tolerance than CPB.

Overall, the research for DMVA provides the ground work for devices that operate on a similar principle. Specifically, a biventricular assist device

was designed and fabricated to advance the procedure for DMVA. Accordingly, there are significant improvements in this device that make it a more viable alternative for circulatory assistance.

3 Mechanical Biventricular Assist Device

A mechanical biventricular assist device (MBAD) that operates similarly to the Anstadt cup has been designed and tested both *in vivo* and *in vitro*. This device consists of a plastic outer shell that internally supports two inflatable bladders. When the device is applied to the heart and the bladders are inflated, compression of the left and right ventricles results. This compression effectively deforms the ventricles and propels blood into the pulmonary and systemic circulation.

The outer shell of the device conforms to the heart and is comprised of distensible polyurethane. The bladders are made of similar polyurethane with slightly different mechanical properties to allow expansion during inflation. They are oriented within outer shell to allow maximum contact with the ventricles during inflation. The shell size is made to fit approximately 4 cm up into the atrial portion of the heart. However, the bladders only encompass the ventricular area of the heart. In order to supply a pathway for air, one 3/16 in (0.5 cm) inner diameter Tygon tube, 12 in (30.4 cm) long, is attached to each of the bladders via the outer shell. Another 12 in (30.4 cm) piece of the same diameter Tygon tubing is attached to the base of the cup to supply negative pressure to the apex of the heart.

3.1 Device Actuation

This device requires either a liquid or gas source to provide bladder inflation. In the past, dichloroflouromethane was used in 12 oz (0.0007 m^3) canisters as a compressed gas source. However, dichloroflouromethane is not approved for clinical use and the canisters do not supply ample volume;

therefore alternate sources of actuation were considered. These included refillable cylinders of helium, nitrogen, and carbon dioxide, and compressed air. An air compressor was chosen as the most viable source of actuation because it was readily available and the large cylinders were too costly. A 1/4 horsepower SpeedAir air compressor was obtained from the Mechanical Engineering machine shop. This compressor has a 10 gallon (0.0378 m^3) accumulator tank and a pressure switch that maintains tank pressure between 20 and 50 psi (95.7 and 239.2 N/m^2). A 50 foot (15.2 m), 1/4 in (0.6 cm) pneumatic hose was fitted with quick connectors and was fastened to a portable pumping unit.

The pumping unit consists of a timer circuit, a three-way solenoid valve, and a pressure regulator rated at 150 psi (717.7 N/m^2). The inlet of the solenoid valve is connected to the gas source, while the two outlets are attached to a vacuum source and to the bladders of the BVAC. The rate of gas delivery is controlled by the timer, while the bladder pressure is controlled through the regulator. During inflation, the solenoid valve opens to the compressed air source; typically, pressures of 3 to 4 psi (14.4 to 19.1 N/m^2) were found to adequately fill the bladders.

The air present in the bladders during inflation is quickly removed by attaching a vacuum source to the outlet port of the solenoid valve. In the past, the air was passively evacuated to the atmosphere. However, this rate of evacuation was extremely slow and was believed to cause impedance to the incoming blood during diastole. Therefore, the rapid evacuation of the bladders with a vacuum source was considered to be a major improvement in device actuation, preserving the normal functionality of the cardiac cycle.

4 Production Process

4.1 General fabrication

The first step in the fabrication process is the construction of a heart replica. This is done by first obtaining a heart, creating a female mold of the heart, and then producing a plastic male mold of the heart. This process has undergone considerable improvement since its inception.

After the mold is created, it is then dipped into two specific mixtures of polyurethane in an extensive dipping process. The end result is a polyurethane MBAD (Figure 4).

4.2 The Molding Process

The replication of a natural heart is created in a series of steps leading to a finished mold. The goal is to obtain a mold of the heart that does not contain any imperfection on its external surface. This allows for ease and accuracy when coating the mold to obtain a reliable and functional MBAD.

The past method for creating a female mold of the heart was through the use of silicone caulking. The heart was suspended within the boundary of a wooden box and silicone caulking was poured into the box using a caulking gun. Unfortunately, due to the high viscosity of silicone rubber, the resultant female replica did not contain enough detail of the actual heart. Therefore, substantial amounts of sanding were required in order to obtain an accurate mold.

In order to obtain a more accurate representation of the heart, microcrystalline, or sculptor's wax, was used as a female mold material. Although machinable wax and paraffin were considered, the expense of

machinable wax and the peeling and cracking associated with the use of paraffin made neither material appropriate for the task.

Once a fresh pig heart was obtained, all of the fat and connective tissue were removed; the pulmonary artery, aorta, vena cava, and pulmonary veins were cut to the level of the left and right atria, and the heart was rinsed with warm water. In order to prevent the heart from collapsing under the pressure generated during the wax molding process, gauze was inserted into all four chambers to maintain rigidity. This also insured that the device would not be made too small for the particular heart size. The heart was then fastened to a nylon string and suspended within the bounds of an appropriate size container.

Next, the wax was liquified by placing it on the burner of an stove. It was discovered that using the minimum temperature to melt the wax was the most effective and accurate way of creating the female replica, so the temperature setting on the burner was placed on low and the wax was heated. Once all the wax was melted, it was carefully poured into the container that enclosed the heart. In order to obtain a seamless parting line in the mold, the wax was poured to a height that corresponded to the widest cross section of the heart and allowed to dry for 120 minutes. The heart was then removed and the top surface of the wax was sprayed with high temperature enamel to create a partition between it and the next layer of wax. The enamel was allowed to dry for several hours. After this, the second layer of wax was poured into the mold and allowed to dry. At this point, the two sections of the female mold were easily separated at the parting line and the heart was removed from the mold. The wax female mold was found to be a near perfect replica of the heart, detailing even the superficial right and left main

coronary arteries (Figure 5). In order to solidify the mold more quickly, the molding container was placed in a refrigerator after the wax was completely poured. The detailed steps required to produce the female mold are outlined in Appendix A.

The process of producing the male mold was much simpler than that for the female mold. Before the female wax mold was taken apart, two adjacent marks were placed on the outer surface of each part of the mold. These marks insured proper alignment of the mold sections when they were reassembled. A hole was placed in the top section of the female mold to allow an entrance for the male mold material. Also, a threaded bolt was suspended within the chamber of the female mold for ease of handling the mold later in the fabrication process. Plaster of Paris was initially used as the molding material, but plastic resin was determined to finish with a much smoother surface and to cure much more quickly than the plaster. This resin was a clear, liquid acrylic plastic mixed with a catalyst hardener. It was used to eliminate the need for coating the mold with a release agent. The pouring was done incrementally, with tapping of the female mold on a hard surface to rid the plastic of air. Once the pouring was complete, the resin was allowed to dry for approximately two hours. Upon extraction from the mold, the contour of the plastic replica was found to be quite accurate and did not require sanding, as did the plaster (Figure 6).

An important step in this process was maintaining the wax mold temperature considerably below ambient temperature to prevent melting during the exothermic reaction between the plastic resin and the hardener. If the wax melts during the process, imperfections in the plastic mold will result. The wax mold was placed in a freezer for 30 minutes and then the

liquid plastic solution was mixed and poured into the mold. The wax mold was then placed in a refrigerator to further prevent wax melting during the reaction. The list of steps required for the production of the male mold are also included in Appendix A.

4.3 Prototypes

Several MBAD prototypes were produced to determine and evaluate device performance. The major limitation of the past design was that it did not maintain its position on the heart even with apex suction. Therefore, two potential solutions were examined. The first employed the use of a ring bladder located at the top portion of the device. This ring bladder inflates first, causing a constriction around the atria and less likelihood of device ejection. This ring bladder was incorporated into the design of several prototypes. However, it was impossible to make the bladder large enough to cause significant clamping around the atrioventricular junction. Therefore, this method was eliminated as a solution for securing the device around the heart.

The second and final prototype utilized the elastic property of the polyurethane of which the cup is made. When removing the cup from the solid mold, the placement of the initial incision in the polyurethane dictates the length of the cup. By making this incision near the threaded bolt that protrudes from the mold, a highly elastic, strong cross section is formed. Since the incision is made near the bolt, this cross section is much smaller than the widest point of the heart. Therefore, in order to fit the cup around the heart, the top portion of the plastic cup must be stretched significantly. After stretching the device and positioning the it on heart, the stretched

material returns to its original cross sectional area. This rubber band effect at the top of the assist device secures the heart within the cup.

A prototype with this design was tested with a fresh heart from a 230 lb (104 kg) pig. It maintained its position on the heart with and without apical vacuum assist. In fact, the device was suspended upside down during operation and it still maintained its position around the heart. This prototype was therefore used for additional *in vitro* testing and for the primary *in vivo* experiment.

4.4 Discussion of Production Advancements

The major disadvantages present in the past process of replicating the natural heart were in molding materials. The female mold was initially made using silicone caulking. Because of its high viscosity, this material does not conform well to the surface of the heart. Three different types of wax and one flexible molding material were investigated as potential replacements for this inadequate material.

The three waxes considered were microcrystalline wax, machinable wax, and paraffin. Because of the high cost of machinable wax and the brittleness of paraffin, microcrystalline wax was used. This wax provides an excellent replication of the surface of the heart, revealing even the details of the superficial coronary arteries.

Additionally, a flexible molding material was considered to effectively replicate heart. It was applied in approximately 30 coats to the heart. Ample dry time was allowed between each coat. When the flexible material was removed from the heart, the result was a fairly accurate female replica. However, this process was lengthy, due to the multiple coatings and the

extensive dry time requirement. Therefore, the flexible mold material was not used in the final mold production process.

Finally, plastic resin was used as a replacement for the plaster of Paris initially used. The plaster required significant dry time and despite attempts to remove the air from the liquid mixture, it was trapped on the surface and caused significant superficial imperfections of the plaster mold. Plastic resin, on the other hand, dries in one to two hours and finishes with a highly smooth surface, requiring little to no sanding. Another important reason for selecting the plastic resin was to eliminate the coating step in the device production process. Since the plaster mold is extremely porous, it requires a coating to seal it from the polyurethane and therefore allow removal of the device from the mold. However, the plastic resin is impermeable to the liquid solvents used in the device production. Therefore, it permits MBAD release and eliminates the need for coating the mold. This reduces production time and simplifies the manufacturing process.

In summary, the device was developed from a preliminary prototype to an effective circulatory assist tool. Changes in both device actuation and design were required in order to accomplish this task. First of all, the newly designed outer shell incorporating the elastic band insured maintenance of the device's position on the heart. Furthermore, the change from environmentally harmful dichlororflouromethane to compressed air as an actuation source made the MBAD safer not only from an environmental standpoint, but also from a clinical one. Finally, the most critical advancement in device design was evacuation of the bladder actively during diastole. This not only facilitated the normal diastolic filling pattern of the heart, but also prevented the life threatening condition of cardiac tamponade

that would surely occur otherwise. Overall, these advancements were necessary for safe and effective MBAD operation.

5 Bench Testing

Various bench tests were performed to evaluate each of the MBAD prototypes. These included a physiological afterload test, a device-heart interaction test, and a durability test.

5.1 Physiologic Afterload Pressure Test

The purpose of this test was to determine whether the MBAD could generate enough ventricular compression to provide physiologic pressure to the systemic and pulmonary circulation. It was accomplished according to the following procedure. First, both the aortic and pulmonary valves of a fresh heart from a 230 lb (104 kg) pig were excised using forceps and a scalpel. Next, the left and right atrium were sutured near the vena cava and pulmonary veins to seal the atrial portion of the heart. Then, aluminum fittings with tapered barbs were connected to the pulmonary artery and aorta with hose clamps. The other side of the aluminum fittings was attached to 3/4 in (1.9 cm) Tygon tubing which was fastened to ports on two plexiglass afterload columns. These columns were designed to provide various amounts of ventricular afterload ranging from 0 to 150 mm Hg. A specific afterload was attained by filling the column to the appropriate height with water.

For this test, the column connected to the right ventricle was filled with 13 in (33 cm) of water to simulate a physiologic afterload of 25 mm Hg. The left ventricular column was filled to a height of 64 in (163 cm) of water to approximate the normal afterload of 120 mm Hg. Once the columns were filled, tubing clamps preventing flow into the ventricles were removed and the water filled each ventricle causing significant dilation. Additional fluid

was then added to each column to replenish the fluid height lost in the ventricles. The 230 lb (104 kg) series MBAD was then inserted onto the heart by carefully stretching the top portion and positioning the device around the heart to maximize ventricular-bladder contact. The apical negative pressure source was then activated and the device assumed a tenacious position around the heart. The portable pumping unit was then switched on at approximately 60 beats per minute (bpm) and the bladder pressure was increased until motion of the fluid columns was observed. This motion corresponded to the compression of the ventricles. Significant fluid motion occurred when the bladder was at approximately 3 psi (14.4 N/m^2). Since left ventricular afterload is much higher than that of the right ventricle, it is clear that this factor determines whether the pump can effectively compress the heart and generate adequate pressure.

This test revealed that at a bladder pressure of only 3 psi (14.4 N/m^2), the MBAD could generate physiologic pressure for both the right ventricle and the left ventricle in an excised pig heart. *In vivo*, the heart is much more compliant and therefore would be more easily compressed. Therefore, it was believed that less bladder pressure would be required to sustain physiologic pressure in a live animal experiment.

5.2 Device-Heart Interaction Test

Most of the bench testing for the several prototypes was done according to visual assessment of the MBAD fit and function on excised pig hearts. These tests were accomplished simply by inserting the heart into the cup and then activating the device with the portable pumping unit. Two key occurrences were anticipated. First, the device's ability to maintain its

position on the heart was determined. This was tested by changing the orientation of the device and the heart with respect to gravity. At the same time, bladder pressure was varied to determine the pressures that would allow the heart to remain in the device. Second, the actual contact between the bladders and ventricles was assessed. This was done by noting the amount of compression of the heart. When the device compressed the heart significantly, deformation of the myocardium resulted in protrusion of the atria from the top of the device. Also, the bladder-ventricle contact area was observed. In each case, the bladders were observed to make full contact with each of the ventricles.

5.3 Durability Test

Each device made was inflated with air from the portable powering device at a rate of 60 bpm with a bladder pressure of 3 psi (14.4 N/m^2). This was done for approximately one hour to investigate potential device failure through the development of air leaks.

6 Animal Experimentation

A primary *in vivo* experiment was performed in order to qualitatively ascertain MBAD performance in an animal. This experiment employed the staff and facilities at the Lehigh Valley Hospital in Allentown, Pennsylvania. Dr. Michael Sinclair performed surgery for the experiment and David Rice assisted in surgery and was responsible for animal acquisition and surgical equipment oranization.

6.1 Preliminary Protocol

In order to prepare for the first animal experiment, a general meeting was held at the Lehigh Valley Hospital. During this meeting, all of the equipment for the experiment was checked and evaluated. This included a 230 lb (104 kg) and a 120 lb (120 kg) series MBAD , the portable pumping mechanism, the vacuum sources, the intraaortic balloon pump (IABP) console, and all surgical equipment. Each MBAD was connected to the pumping mechanism and the bladders were observed to inflate fully, making contact in the center of the cup. At the suggestion of the surgeon, the IABP console was connected to each device. However, it only supplied a 40 mL maximum air volume, which was inadequate for bladder inflation in either device, as previously measured. Therefore, this console could not be used as a pumping source. Finally, the two wall vacuum sources were verified to supply ample negative pressure to accomplish bladder evacuation and device position maintenance.

All surgical equipment was obtained and accounted for. The cardiac surgeon and laboratory director discussed the different options for exposing the heart and decided upon a procedure known as a thoracotomy.

The size of pig to be used in the experiment was also determined. The cardiac surgeon and animal researcher concluded that a 230 lb (104 kg) pig would be cumbersome in the operating room. Therefore, it was agreed to work with a 120 lb (54 kg) pig.

6.2 The Primary Animal Experiment

The first animal experiment occurred at the Lehigh Valley Hospital in the animal surgical suite. The 120 lb (54 kg) pig arrived pre-anesthetized with acepromazine maleate, administered intramuscularly in a 1.0 mg/kg dosage. Induction of the pig was performed using ketamine HCL at a dosage of 25 mg/kg. The animal was placed on the operating table and all four legs were secured. An endotracheal tube was then inserted into the animal and it was enflourane aspirated with 20% nitrous oxide in oxygen. Also, an IV pentobarbital solution was administered at 10 mg/kg.

Before the animal's chest was opened, a Swan-Ganz catheter was inserted through the iliac vein into the right ventricle in order to measure central venous and right ventricular pressure. The Swan-Ganz catheter is a quadruple lumen catheter used to monitor hemodynamics during surgery. Once the catheter is inserted into the iliac vein, a balloon at its tip is inflated and blood returning to the heart drags its distal port into the right ventricle. This port is connected to a fluid filled pressure transducer and measurement of right ventricular pressure is obtained. The proximal port is located several

centimeters away from the distal and is therefore positioned to supply inferior vena cava pressure.

A thoracotomy was performed in order to expose the animal's heart. An incision was made between the fourth and fifth ribs and the connective tissue was removed. A periosteal elevator was used to fully expose the ribs. A rib retractor was utilized to make the heart accessible through the intercostal space.

Unexpectedly, the size of the heart of the 120 lb (54 kg) pig was larger than anticipated. Generally, an excised heart is smaller than an intact heart. However, the degree of difference in size was not realized until the heart of this animal was exposed. The intact heart was nearly twice the size of the excised heart obtained from the butcher. This is attributed to the dilation of the heart during diastole, the proliferation of the heart muscle with blood, the coronary circulation, and perhaps even the muscle tone due to continuous myocardial electrical activity. Therefore, the 230 lb (104 kg) series MBAD was used to accommodate the larger size heart.

Next, the heart was fibrillated, and the device was applied. At this time, the negative pressure was applied at the apex, not at the outlet port of the solenoid valve. The SpeedAir air compressor was connected to the the bladders through the Tygon tubing. The pumping cycle was begun at 60 bpm while the bladder pressure was regulated from 3 to 4 psi (14.4 to 19.1 N/m^2). The device was operated for 30 minutes in this mode. The device maintained its position on the heart quite tenaciously and sufficiently compressed the ventricles throughout this range of bladder air pressure. However, the slow rate of bladder evacuation was confirmed to prevent efficient fill of the heart. Therefore, the negative pressure source was switched on at the outlet port of

the solenoid valve to cause active bladder evacuation. Again, the device was operated for 30 minutes with bladder pressures ranging from 3 to 4 psi (14.4 to 19.1 N/m^2). In this case, the rate of air evacuation from the bladders was rapid and therefore refill of the heart was unimpeded.

At the conclusion of the experiment the animal was euthanized with a 50 mg/mL dosage of sodium pentobarbital solution.

6.3 Discussion and Observations

The purpose of this experiment was to determine the most optimal surgical procedure for device application and qualitatively assess the device's function as a circulatory assist tool. The device was applied to the fibrillating heart of the animal for a period of approximately 1 hour. It was observed to continually maintain its position on the heart and fully compress the ventricles, causing significant ejection of blood. This was noted by the aortic pulse following bladder inflation.

The deflation of the bladders was observed to be quite rapid with the assist of the vacuum source, not causing any impedance to diastolic fill. A seal between the device and the heart along the atrioventricular junction resulted in negative pressure on the ventricular walls.

An important consideration in the experiment is the size of the animal. This factor dictates the complexity of the procedure. In this particular case, there was some difficulty in obtaining pressures with the Swan-Ganz catheter due to the complicated anatomy of this large animal. By choosing a smaller pig, catheterization of the heart and the surgical procedure would have been simpler and less time-consuming. This would allow more time for useful data acquisition.

The surgical procedure used in this experiment was a thoracotomy. However, this procedure does not allow much working space around the heart, and it therefore made device application difficult. A more effective way to expose the heart would be to employ a surgical procedure known as a median sternotomy. In this procedure, the sternum is cut and retracted, allowing greater access to the heart.

The IABP console should be considered as a potential powering device for the MBAD due to its high speed of gas delivery to and from the device. Its maximum stroke volume is only 40 mL, but with certain internal modifications, it could be utilized as an improved pumping mechanism.

The process of attaching the device to the intact heart is in need of improvement. In the experiment, the two-handed method was revealed to be very cumbersome and time consuming. It could be replaced by using a large, blunt end retractor to spread the top portion of the device for application around the heart. The use of the retractor would eliminate the need to crowd the hands around the heart, decreasing the overall surgical time and the chance of damage to the internal organs.

7 General Discussion of the MBAD

7.1 Advantages over Common Forms of Assist

This device has several advantages over currently available circulatory assist devices. First of all, its operation does not necessitate blood contact. This advantage is extremely significant since two of the major obstacles that other assist devices face stem from blood contact, namely hemolysis and thrombogenesis. For example, the complex fluid mechanics of blood flow makes the design of rotary pumps quite challenging. At any point in operation, if a stagnation point develops either in the pump housing or in the cannulae connecting the pump to the circulatory system, thrombogenesis can occur. This emboli can either clog the pump or it can break off and lodge in the brain, kidneys, or lungs, causing severe damage to these vital organs. This can be fatal to the patient. This same problem of thrombogenesis is seen in assist devices with pneumatically compressed blood sacs and artificial valves.

Furthermore, many of the blood-contacting assist devices require continuous anticoagulation therapy. This is accomplished through the use of either heparin, persantine, or coumadin. The application of these anitcoagulants increases the chance of severe bleeding due to accidental cuts.

Another advantage of the BVAC is that it assists circulation by maintaining the physiologic pulsatile flow requirement. Centrifugal assist devices are notorious for end organ dysfunction when used for long term assistance due to the non-pulsatile flow input to the systemic circulatory system.

Another important advantage of the MBAD is the ease with which it is applied. Since it is simply a semi-rigid shell that fits securely around the heart, it can be applied in a matter of seconds. This significantly reduces surgery time and therefore would allow the patient a much higher chance of survival. This is especially evident when considering the significant time involved in performing complex surgical techniques for anastomoses of rotary pump inlet and outlet cannulae. Also, the MBAD's simplicity of operation limits the amount of technical problems that can occur *in vivo* when compared to devices that operate based on complex circuitry and mechanical motion.

Finally, the insignificant cost and ease of production of this device set it apart from all others in its class.

7.2 Advantages over the Anstadt Cup

This device and the Anstadt cup have several commonalities, but the changes in design for this device have resulted in several advantages over the Anstadt design.

Because Anstadt's device consists of a rigid outer shell, it requires surgery for removal. However, some patients cannot survive a second thoracotomy. In order to eliminate the need for this traumatic surgery, the outer shell of the BVAC is created with a flexible polyurethane to allow device removal through a large thoracotomy tube.

By making the outer shell flexible, injury to the fragile internal organs surrounding the heart would be prevented; this type of injury could occur if the patient was moved around significantly with the rigid shell implanted. In fact, Skinner [3] demonstrated multiple cases of damage to the heart and

lungs through contact with the rigid device. The deformable outer shell also allows a much closer fit to the size of the heart, and therefore would tend to reduce the overall shear stress on the ventricles.

Furthermore, in order to simulate physiologic conditions as closely as possible in a fibrillating heart, the rate of inflation and deflation of the bladders can be monitored. That is, the normal human heart spends 70% of its time in diastole and 30% in systole. By adjusting the timer circuit of the portable pumping unit, the device can be made to mimic this systolic phase ratio through the inflation-deflation cycle. In a moderately dysfunctional heart, the inflation and deflation of the device would be synchronized with the ECG through a pacemaker.

Once the device is applied to the heart, it creates a seal just past the atrioventricular junction, due to the design change. This seal provides a vacuum chamber that surrounds the entire heart. This can produce active diastole of the heart and greater end-diastolic volume. Starling's law of the heart states that increased end-diastolic volume causes greater myocardial wall tension and therefore more forceful contraction. This means that an increased volume of blood can be pumped during one cycle than if the pump was not used. This active diastole is not a characteristic of many circulatory assist devices and it is believed to offer several advantages to the dysfunctional heart.

7.3 Active Diastole

According to William Grossman, "Many of the signs and symptoms of cardiac failure, previously attributed to impaired systolic performance, may be due in large part to altered diastolic properties of the ventricular chambers"

[19]. One important function of the MBAD that deserves careful consideration is its ability to provide negative pressure to the walls of the ventricle throughout the cardiac cycle. This negative pressure could assist ventricular diastole in several ways.

Because of the negative pressure applied to the myocardium, the left and right ventricular chamber pressures would attain negative values during diastole. This negative pressure could result in an increased flow rate of blood into the ventricles and a higher end-diastolic volume. This means that for each actuation of the ventricular walls, a larger stroke volume will be supplied to the aorta and pulmonary artery. This allows a lower heart rate and more time for the dysfunctional heart to unload and recover. The amount of this recovery can be controlled through regulation of the negative ventricular wall pressure.

The negative pressure applied to the ventricular walls could also augment coronary perfusion. During diastole, the pressure in the coronary arteries located in the ventricular walls attains the same pressure as does the ventricular chambers. With negative pressure applied to the walls of the myocardium, this diastolic chamber pressure decreases. The coronary os, located in the aorta directly distal of the aortic valve, undergo systolic pressure during contraction. With the application of suction to the myocardium, the pressure gradient driving flow from these openings into the coronary circulation is greater. Therefore, coronary blood flow rate increases, delivering more oxygen to the potentially damaged myocardium.

7.4 Considerations

The two major concerns in the device design are the prevention of cardiac tamponade and adequate device fit to insure vacuum seal and proper contact between the ventricles and bladder.

Pericardial tamponade occurs when the pericardium secretes abnormally high amounts of fluid around the heart. This fluid constricts the heart and prevents proper diastolic fill. The MBAD could cause this same type of problem if it is not designed large enough to allow significant dilation of the heart during diastole.

The length of the MBAD is crucial in forming the vacuum seal that preserves the negative ventricular epicardial pressure during diastole. This length must be made to allow geometric alignment of the top portion of the device with the atrioventricular junction. Also, the bladders must be formed to allow complete contact and full ventricular compression during inflation.

8 Myocardial Mechanics

8.1 Introduction

An *in vivo* experiment that directly quantifies the function of the MBAD is of primary importance in advancing the device toward clinical use. A rapidly growing area of research in cardiac physiology and biomechanics that directly relates to *in vivo* MBAD testing is the study of deformation of the myocardium during ventricular contraction. Although this area of research is relatively new, it provides insightful ideas for quantifying the hemodynamic performance of the MBAD. Moreover, a thorough knowledge of the specifics of myocardial deformation allows an advanced understanding of the design requirements of the MBAD.

8.2 Background

Various methods have been postulated in the literature for measuring myocardial deformation in an intact heart. One method by Waldman [19] involves the implantation of lead beads in the myocardium. This method utilizes high-speed biplane cineradiography to track the motion of these implanted beads. The beads are positioned in the heart, implanted from the epicardium to the endocardium. Three closely-spaced columns of four to six beads were implanted within the ventricular wall. Five additional beads were implanted on the epicardium, three above each column, one at the bifurcation of the left main coronary artery, and one at the apical dimple. ECG, left ventricular pressure, and aortic pressure were recorded during high speed simultaneous biplane cineradiography (16 mm, 120 frames/second).

The camera shutter marks were also recorded to allow correlation between the cine frames and the physiological events.

The heart was excised after the animal was sacrificed and a calibration grid was positioned on the left ventricle in each projection plane. This was to provide a basis for three-dimensional x-ray measurements. The shadows of each of the marker's centroids caused by the x-rays were captured through two dimensional digitizing. Three-dimensional x-ray coordinates were then obtained. By utilizing the reference markers on the epicardium these x-ray coordinates were converted to cardiac coordinates.

Strain was calculated by forming finite tetrahedrons of markers within the ventricular wall. The base was comprised of three markers that were all within 1 mm difference of depth beneath the epicardium. The vertex was between 1.9 and 4.0 mm from the base. The strain was calculated from the formula

$$\delta s^2 - \delta s_o^2 = \sum_{i=1}^{3} \sum_{j=1}^{3} 2E_{ij}\delta a_i \delta a_j$$

where E_{ij} is the symmetric strain tensor. This is related to δs, the distance between markers before contraction and δs_o, the distance between markers after contraction. The a_n coordinates represent the dimensions of the original tetrahedron.

8.3 Dynamic Tracking of the Myocardium

Aside from the method of Waldman [19], another procedure for determining patterns of ventricular wall deformation has been developed. This method, performed at Allegheny General Hospital in Pittsburgh,

Pennsylvania, involves the placement of ultrasonic crystals on the myocardium in order to measure cardiac motion. It is significantly less time consuming than Waldman's method and can be used to accurately describe myocardial deformation. This experiment could potentially be used to quantify the performance of the MBAD.

8.31 Materials and Methods

A mongrel dog was anesthetized and maintained through an endotracheal aspiration of halothane. A median sternotomy was performed and a rib spreader was utilized by the surgeons to expose the heart. Pulse transit ultrasonic dimension gauges were attached to six locations on the heart to provide three-dimensional tracking of the heart, as shown in Figure 7. The three pairs of transducers were positioned to measure the long axis, the short axis, and left ventricular wall thickness of the heart. The first pair was placed at the widest section of the epicardium to measure the short axis. The second pair was sutured at the apex and base to capture long axis changes in dimension during contraction. Finally, the third pair was placed on the epicardium and on the endocardium through a needle hole.

These crystals receive and send pulses of ultrasound in pairs. The transit time of the pulse between the piezoelectric transducers is measured as an analog signal. This signal is directly proportional to the distance between the crystals. The sonomicrometer sampling rate is 1000 Hz.

The crystals' analog output is sent to an oscilloscope and is calibrated into distances. Baseline heart dimensions are recorded on an IBM data acquisition program. One to four weeks after implantation, the dog was studied while conscious. If it was determined to be healthy, it was given a

general anesthetic in order to remove the transducer leads from an abdominal pouch. The leads were then connected to the sonomicrometer. Left ventricular pressure was measured by inserting a Millar PC-350 micromanometer into the left ventricle through the carotid artery. Right ventricular pressure was measured by a Swan-Ganz catheter.

All data were recorded through a real-time data acquisition program. After the dog was sacrificed, the position of the ultrasonic crystals was verified to have remained unchanged throughout the experiment.

8.32 Analysis of data

The left ventricle was geometrically modelled as a three-dimensional prolate ellipsoid, since the long axis diameter is 30-40% greater than the short axis. Spherical models have been used in the past, but have been found to underestimate circumferential stress [20]. The shell thickness at the apex and base was assumed to be 55% of the midwall thickness as found by Rankin [21]. The equation for the volume of a prolate ellipsoid is

$$V = \pi/6(b-2h)^2(a-1.1h)$$

where b is the short axis dimension, a is the long axis dimension and h is the wall thickness [21]. Three pressure-volume curves were calculated from the ultrasonic dimension data and the pressure utilizing an IBM cardiovascular analysis program (Figure 8).

8.33 Results

The changes in pressure, short axis, long axis, and wall thickness are shown in Figure 9. These data reveal shortening of both the long and short axis during ventricular contraction. They also demonstrate that the wall thickness increases during contraction. This can be seen in the short axis dimension plot, which varied from 6.15 cm at end diastole to 5.72 cm at end systole. The long axis dimension varied form 7.75 cm to 7.53 cm between end diastole and end systole. Finally, the wall thickness varied from 1.5 and 1.85 cm between end systole and end diastole. Longitudinal, radial, and circumferential strain were calculated at each point in the cardiac cycle using the relation

$$\varepsilon=\ln (X/X_0),$$

where X_0 is the end-diastolic dimension. X is a general variable representing each of the three dimensions. For circumferential strain, X becomes L and

$$L=\pi(b-h) \text{ and } L_0=\pi(b_0-h_0)$$

were used to calculate the circumference at each time during the cardiac cycle [21]; L_0 is the end-diastolic circumference. These strains are shown in Figure 10. The average stroke work is calculated over three of the cardiac cycles and is defined as the average area enclosed by the three pressure-volume curves (Figure 8). It was found to be approximately 1204 g-cm.

8.34 Discussion

This method of determining myocardial deformation results in the strain values (Figure 10) similar to those found by Waldman [19]. The corresponding plots of circumferential, longitudinal, and radial strain found by Waldman are shown in Figure 11. As is evident from these plots, the discrepancy in strain values is very small. For instance, the maximum circumferential strain determined by Waldman is -0 .17. The present method predicts this value to be -0.16. For longitudinal strain, both methods predict values near -0.025, Finally, radial strain reaches a value of 0.20 predicted by Waldman and 0.18 from the ultrasonic data.

Although these two experiments were obviously performed on different animals, virtually identical trends in strain are evident. Therefore, the data confirms that this method of determining dynamic left ventricular geometry is as effective as the method utilizing high-speed biplane cineradiography with lead bead markers. However, this experiment is much simpler and less time consuming than Waldman's experiment.

The pressure-volume curve generated from this data demonstrates that values of stroke work for baseline cardiac output can be determined. The MBAD should cause several changes in the pressure-volume loop. First, since the MBAD applies negative pressure to the walls of the left ventricle, it should produce a significantly lower diastolic pressure. Therefore, the rapid filling phase, point four to point one in Figure 8, should occur at a much lower pressure.

By adjusting the device bladder pressure, the end-systolic volume can be regulated. A high bladder pressure causing a large ventricular compressive force results in a reduction in end-systolic volume. By increasing negative

pressure on the ventricles during diastole, a large end-diastolic volume will result. Finally, increases in systolic pressure will also accompany the increased compressive force on the ventricles.

In a patient requiring assist, end-systolic volume is high and the systolic pressure is low. With the addition of the MBAD, the ejection fraction and the systolic pressure should be augmented. This should produce a pressure-volume curve with lower end-systolic volume and higher systolic pressure, as shown in Figure 8. It is obvious from this curve that the stroke work should increase significantly with the application of the MBAD. Therefore, this device should augment hemodynamic performance and unload the ventricles.

In conclusion, this method is believed to be the simplest, most effective way of quantifying the performance of the MBAD. By implanting ultrasonic crystals on an intact animal heart and measuring ultrasonic dimension changes during contraction with and without the MBAD, an extremely effective measure of the device's performance can be obtained.

9 Mechanical Interaction of the MBAD Bladder and the Heart

9.1 Introduction

An essential consideration in the design and application of the MBAD is its mechanical interaction with the heart; this determines the life of the bladder and the effects on the myocardium. Because of the repetitive nature of the MBAD application, a poorly designed bladder could result in early failure and/or myocardial necrosis.

When the bladder inflates and pushes into the heart, it becomes loaded by the heart. Due to the complexity and present uncertainty of myocardial mechanics, it is difficult to pinpoint the form of cardiac loading. For instance, the right ventricle differs from the left ventricle in dimensions, contractile patterns, and internal pressure. These differences will certainly result in different loading conditions on the bladder. Additionally, a heart with noncontractile, infarcted tissue may cause irregularities in bladder loading and stress concentrations.

A convenient and logical method for analysis of the interaction between the heart and bladder employs the use of shell theory. This allows calculations of stress, strain, and deformations of the bladder using various models of cardiac loading. In this way, it is possible to analyze the interaction of the bladder with the heart under a variety of loading scenarios. As a first approximation, the MBAD bladder will be modelled as a portion of a thin-walled spherical shell of revolution, quasistatically loaded by the heart. As shown in Figure 12, the shell representing the MBAD bladder can be formed by rotating a curve (meridian) about an axis in its own plane, where ϕ represents the meridional angle and each θ, the azimuthal angle, defines a

unique meridian. A element of this shell is depicted in Figure 13 and the differential equations that result from an equilibrium analysis on the shell are:

$$\partial/\partial\phi\,(rN_\phi) + r_1\,(\partial N_{\phi\theta}/\partial\theta) - r_1 N_\theta \operatorname{Cos}\phi + p_\phi r r_1 = 0 \qquad 9.1.1$$

$$\partial/\partial\phi\,(rN_{\phi\theta}) + r_1\,(\partial N_\theta/\partial\theta) + r_1 N_{\theta\phi} \operatorname{Cos}\phi + p_\theta r r_1 = 0 \qquad 9.1.2$$

$$N_\phi/r_1 + N_\theta/r_2 = p_r \qquad 9.1.3$$

where equation 9.1.1 is a force balance in the ϕ direction, equation 9.1.2 is a force balance in the θ direction, and equation 9.1.3 represents equilibrium for forces which are perpendicular to the shell element [23]. The shear stress resultant is defined as $N_{\phi\theta}$. N_ϕ and N_θ are the stress resultants in the ϕ and θ directions; they are defined as positive in directions of increasing angles. Each of these stress resultants is defined as the stress per unit length of the shell thickness. Once these stress resultants are calculated, it is possible to obtain the shell stresses by dividing each of the resultants by the bladder thickness, t. Therefore, information regarding bladder failure based on comparison with the critical stress for this material is obtained.

Several different loading schemes will be used to approximate the interaction between the heart and the MBAD bladder. These loadings are characterized by symmetry and non-symmetry with respect to the shell axis. Axisymmetric loads result in shell displacements that are independent of the azimuthal angle, θ. Non-symmetric loads, however, cause displacements that are dependent upon the θ.

9.2 Axisymmetric Load Models

A typical description of an axisymmetric load model for the MBAD bladder involves fixing the loading pressure to a maximum value where the bladder extends furthest into the myocardium during inflation and to zero at its edges. Two suitable representations for this are a meridional angle dependent pressure loading and a myocardial displacement-proportional model.

Meridional Angle Dependent Loading

Axisymmetric loads, loads which are symmetric about the shell axis (Figure 12), are widely studied and present fairly straightforward solutions for stress, strain, and deformation of the shell element. In this case, all derivatives with respect to θ are zero; therefore, the equations of equilibrium, 9.1.1 and 9.1.3, reduce to:

$$\partial(rN_\phi)/\partial\phi - r_1 N_\theta \operatorname{Cos}\phi = -p_\phi r\, r_1 \qquad 9.2.1$$

$$N_\phi/r_1 + N_\theta/r_2 = p_r \qquad 9.2.2$$

Equation 9.1.2 describes torsion about the shell axis and will be neglected in the present analysis by assuming $N_{\phi\theta}=0$. The meridional angle dependent form of axisymmetric loading will allow for a maximum loading at the apex of the bladder where the heart is deformed the most and will diminish to zero loading at the edges of the spherical shell bladder. It will incorporate the constant internal pressure of the bladder supplied by the portable pumping unit. One function that models these criteria is $P_r=A \operatorname{Cos}\phi - P_o$, where P_r is

the force per unit area normal to the surface of the bladder, P_o represents internal bladder pressure, and A is the amplitude, defined by the mechanics of the myocardium. With this pressure loading, we see that at $\phi=0$, the pressure is maximum. Furthermore, it is assumed that $P_\theta=0$ and $P_\phi=0$. By substituting 9.2.1 into 9.2.2, we obtain

$$N_\phi = (1/r_2 \sin^2\phi)\int_0^\phi r_1 r_2 P_r \cos\phi' \sin\phi' d\phi' \qquad 9.2.3$$

After substituting Pr into 9.2.3 and integrating, the stress resultants for a spherical shell of radius r=a are

$$N_\phi = a\,[\,(A/3\sin^2\phi)(1-\cos^3\phi) - P_o/2] \qquad 9.2.4$$

$$N_\theta = a\,[\,-(A/3\sin^2\phi)(1-\cos^3\phi) - P_o/2 + A\cos\phi) \qquad 9.2.5$$

Qualitative measurement has revealed that ϕ extends to approximately $\pi/4$. These expressions for the stress resultants can be better understood by gaining physical insight into their effects on the shell. For N_ϕ, the limit as ϕ tends to zero is $(a/2)(A-P_o)$. This value can be demonstrated to be correct by balancing forces on a small circle near the apex of the bladder, where ϕ is approximately zero. The radius of this small circle is $(a \sin\phi)$ and its area is therefore $\pi a^2\sin^2\phi$. The total vertical pressure loading on the circle near the apex is (A-Po). The vertical component of the meridional stress, $N_\phi \sin\phi$ multiplied by the length of the circle, $2\pi a\sin\phi$, gives the total vertical force resisting the pressure loading. Dividing this force by the circular area and solving for N_ϕ,

the limiting value as ϕ tends toward zero in equation 9.2.4 is verified. N_θ also approaches $(a/2)(A-P_o)$ as ϕ tends toward zero.

The strains are derived from the stresses by utilizing Hooke's law. They are given by the formulas

$$\varepsilon_\phi = (1/Et)\,(N_\phi - \upsilon N_\theta) \qquad 9.2.6$$

$$\varepsilon_\theta = (1/Et)\,(N_\theta - \upsilon N_\phi) \qquad 9.2.7$$

where E is Young's modulus of the bladder material, t is the shell layer thickness (bladder thickness), and υ is Poisson's ratio for the bladder. Substituting the values for stress, the formulas for strain are

$$\varepsilon_\phi = (a/6Et)\,\mathrm{Sin}^2\phi\,[\,2A(1-\mathrm{Cos}^3\phi)(1+\upsilon) - 3P_o\mathrm{Sin}^2\phi(1-\upsilon) - 6A\upsilon\mathrm{Sin}^2\phi\mathrm{Cos}\,\phi] \qquad 9.2.8$$

$$\varepsilon_\theta = (a/6Et)\,\mathrm{Sin}^2\phi\,[\,-2A(1-\mathrm{Cos}^3\phi)(1+\upsilon) - 3P_o\mathrm{Sin}^2\phi(1-\upsilon) + 6A\upsilon\mathrm{Sin}^2\phi\mathrm{Cos}\,\phi] \qquad 9.2.9$$

Both strains tend to the same value, $(a/2Et)(A-Po)(1-\upsilon)$, as ϕ approaches zero; this is expected based on the behavior of the stresses. The displacements can be calculated based on their geometric relationship with the strain [23]. v represents displacement tangent to the meridian, u is displacement tangent to the parallel circle, and w is displacement normal to the shell surface. u and v are positive in directions of increasing angles and w is positive when directed outward from the shell surface. The displacement v is given by

$$v=\int_0^{\phi} a(\varepsilon_\phi-\varepsilon_\theta)/\sin\phi'\, d\phi' \qquad 9.2.10$$

Substitution of the strains and integration gives the final solution,

$$v=(Aa^2(1+\upsilon)/3Et)\,[-\cot\phi+\cot\phi\cos\phi+ \log(2(1-\cos\phi)/\sin^2\phi)\sin\phi] \qquad 9.2.11$$

A plot of $v/(Aa^2/3Et)$ versus ϕ is created (Figure 14) by substituting an approximate Poisson's ratio, $\upsilon=0.5$, for the elastomeric polyurethane bladder. The displacement normal to the shell surface, w, is

$$w=a\,\varepsilon_\phi - v\cot\phi \qquad 9.2.12$$

and, substituting,

$$w=(a^2/6Et)\,[-(2A(1-\cos^3\phi)/\sin^2\phi)(1+\upsilon)-3P_o(1-\upsilon)+6A\cos\phi] - (Aa^2(1+\upsilon)/3Et)\,[-\cot^2\phi+\cot^2\phi\cos\phi+\log(2(1-\cos\phi)/\sin^2\phi)\sin\phi] \qquad 9.2.13$$

The plot of the this displacement (Figure 15) with $\upsilon=0.5$ is formed by subtracting $Po(a^2/4Et)$ from w and dividing this result by Aa^2/Et. Since Po=3psi ($2.1 \times 10^4 N/m^2$), E=1.6psi ($1.1 \times 10^4 N/m^2$), a=2.5in (6.35cm), and t=.012in (0.03cm), a general plot normalized in A is formed. E is calculated from the stress-strain material specifications for the B. F. Goodrich Estanes that comprise the MBAD bladder. There is no displacement in the u-

direction for the axisymmetric case because it represents non-symmetric behavior.

From the plots of the displacements several interesting points are noted. First, as ϕ approaches zero v tends toward zero. This demonstrates that there is no meridional displacement at the apex of the bladder. This makes physical sense since a purely symmetric loading will cause no motion of the apical point relative to the shell axis. Additionally, it is observed that the meridional displacement increases positively with increasing ϕ; this is seen physically by viewing the bladder in its loaded and unloaded state. If one hypothetical point on the shell surface is observed as it shifts from the unloaded to the loaded state, it is obvious that in the loaded state, the point corresponds to a larger meridional angle than it did in the unloaded state. This positive shift in the meridional angle implies a positive meridional displacement. Furthermore, the change in relative meridional angle positions of the hypothetical point is seen to grow as ϕ increases.

The plot of the displacement normal to the shell (Figure 15) reaches values of 0.5 and 0.16 at ϕ=0 and $\pi/4$, respectively. These values are reasonable and they define the actual shape of the surface of the shell.

It is interesting to note that the normal displacement depends on the internal bladder pressure, whereas the meridional displacement does not. This agrees with intuition, since higher internal bladder pressures certainly will affect the normal displacement of the shell during loading. This is not the case for the meridional displacement, where changing bladder pressure between the shell's loaded and unloaded state causes no change in the meridional angle.

Myocardial Displacement-Proportional Loading

Another possible model of axisymmetric loading assumes that the pressure loading on the bladder is directly proportional to the displacement of the heart. Figure 16 represents the relationship between the radius of curvature of the bladder, a, and the radius of curvature of the heart, b, before and after compression of the heart. Curve 1 represents the undeformed heart and the deflated bladder; Curve 2 shows the inflated bladder and the deformed heart. Here, Pr, the pressure normal to the bladder, can be represented as $k(a-r_o(\phi))$, where k is a constant and $(a-r_o(\phi))$ denotes the displacement of the heart as it is deformed by the bladder. This representative loading describes maximum pressure loading at $\phi=0$ and zero pressure loading at the bladder edges where $\phi=\phi_o$. $r_o(\phi)$ is determined through the geometrical relationship between the two circles that correspond to the shape of the bladder and the heart (Figure 16). Depending on the bladder design, this relationship is fixed by ϕ_o, a, and b. ϕ_o defines the maximum value of ϕ for the bladder. For this model, ϕ_o will be approximated as $\pi/4$. After extensive trigonometric manipulation (Figure 16),

$$r_o(\phi) = X + b\phi/\mathrm{Sin}\,\phi \qquad 9.2.14$$

where

$$X = [a^2 + b^2 - 2ab\,\mathrm{Cos}(\pi - (\phi_o + \mathrm{Sin}^{-1}((\mathrm{Sin}\,\phi_o)a/b)))]^{1/2} \qquad 9.2.15$$

Now, substituting Pr into equation 9.2.3, the stress resultants in the ϕ and θ directions are

$$N_\phi = ak\,[\,(a-X)/2 - b\,(\cos\phi + \phi\sin\phi - 1)/\sin^2\phi\,] \qquad 9.2.16$$

$$N_\theta = ak\,[\,(a-X)/2 + b\,(\cos\phi - 1)/\sin^2\phi\,] \qquad 9.2.17$$

The limit of each of the stress resultants as ϕ approaches 0 is $(a-b-X)/2$. As in the previous axisymmetric case, this limit is verified by performing a force balance on a small circle at the apex of the bladder where ϕ tends toward 0. The strains are calculated again by using equations 9.2.6, and 9.2.7.

$$\varepsilon_\phi = (ak/Et)\,[\,(a-X)(1-\upsilon)/2 - b\,(\cos\phi - 1)(1+\upsilon)/\sin^2\phi - b\phi/\sin\phi\,] \qquad 9.2.18$$

$$\varepsilon_\theta = (ak/Et)\,[\,(a-X)(1-\upsilon)/2 + b\,(\cos\phi - 1)(1+\upsilon)/\sin^2\phi + \upsilon b\phi/\sin\phi\,] \qquad 9.2.19$$

Each strain value converges to $ak(1-\upsilon)(a-b-X)/2Et$ as ϕ approaches 0. Substitution of the strains into 9.2.10 and 9.2.12 gives the deformations,

$$v = (ba^2k(1+\upsilon)/Et)\,[\,-\csc\phi - \sin\phi\,\log(1-\cos\phi)/\sin^2\phi + \cot\phi - \cos\phi + \sin\phi\,] \qquad 9.2.20$$

$$w = (a^2k/Et)\,[\,((a-X)(1-\upsilon)/2) + \upsilon b\phi/\sin\phi + b(1+\upsilon)(-1/\sin^2\phi - \cos\phi\,\log(1-\cos\phi)/\sin^2\phi + \cot^2\phi - \cos\phi\cot\phi + \cos\phi)\,] \qquad 9.2.21$$

The plot of v is shown in Figure 17. It is obtained by substituting υ=0.5 and normalizing by dividing with ba^2k/Et; in this way, it is not necessary to determine k. This meridional displacement behaves similarly to the meridional displacement in the previous axisymmetric analysis. It converges to zero as ϕ approaches 0 and it increases as ϕ becomes larger. The plot of displacement normal to the shell, shown in Figure 18, is formed by assuming a ratio of 2:1 between the radius of the bladder circle and the radius of the myocardial surface, ie. a/b=1/2. w is divided by a^2k/Et to normalize the plot. From the plot, w reaches approximately 0.97 at ϕ=0 and 0.4 at $\phi=\pi/4$. As in the previous axisymmetric case, there is no azimuthal displacement, u. Furthermore, this behavior for axisymmetric loading complies with physical intuition.

9.3 Non-symmetric Loading Model

The two previous models of axisymmetric loading represent potential myocardial loadings on the MBAD bladder. However, if the MBAD was applied in a situation where a portion of the heart was infarcted or dysfunctional, the pressure loading pattern of the heart on the bladder may not be symmetric with the axis through the center of the bladder (Figure 12). In fact, the extensive thickness of the left ventricular wall near the apex of the heart may result in a natural non-symmetric loading on the bladder. In this case, the bladder load may not only vary with the meridional angle but also with the azimuthal angle, θ. An analysis of non-symmetric bladder loading, perhaps representing more realistic physiologic behavior, will be performed. This analysis will be viewed as an addition to the axisymmetric loading of the bladder. That is, solutions for the axisymmetric case and the non-symmetric

case can be added to give an overall solution for the mechanical behavior of the bladder undergoing both symmetric and non-symmetric loading.

The two previous models of axisymmetric loading of the MBAD bladder by the heart are fairly straight forward derivations. However, the non-symmetric case requires a more sophisticated approach. For the solution of the non-symmetric case the normal pressure loading on the bladders will be modelled as $Pr=-B \sin\phi \cos\theta$, with $P_\phi = 0$ and $P_\theta = 0$ again. ϕ ranges from 0 to ϕ_0 and θ varies from 0 to 2π. This case will incorporate increased pressure loading on the bottom side of the heart, $\theta=\pi$, and decreased loading at the top of the heart, $\theta=0$ (Figure 12). The governing equations are obtained from 9.1.1-9.1.3. For this case, 9.1.3 is used to eliminate N_θ from equations 9.1.1 and 9.1.2. The following solution for the stress resultants are obtained [23]:

$$N_\phi = -\cos\theta\,(Ba/3)\,[(2+\cos\phi)(1-\cos\phi)\cos\phi/(1+\cos\phi)\sin\phi] \qquad 9.3.1$$

$$N_{\phi\theta} = -\sin\theta\,(Ba/3)\,[(2+\cos\phi)(1-\cos\phi)/(1+\cos\phi)\sin\phi] \qquad 9.3.2$$

$$N_\theta = -\cos\theta\,(Ba/3)\,[(3+4\cos\phi+2\cos^2\phi)(1-\cos\phi)/(1+\cos\phi)\sin\phi] \qquad 9.3.3$$

Now, the strains can be calculated from equations 9.2.6 and 9.2.7

$$\varepsilon_\phi = -\cos\theta\,(Ba/3Et)\,((1-\cos\phi)/((1+\cos\phi)\sin\phi))\,[\cos\phi(2+\cos\phi)-\upsilon(3+4\cos\phi+2\cos^2\phi)] \qquad 9.3.4$$

$$\varepsilon_\theta = -\cos\theta\,(Ba/3Et)\,((1-\cos\phi)/((1+\cos\phi)\sin\phi))\,[(3+4\cos\phi + 2\cos^2\phi)-\cos\phi(2+\cos\phi)] \qquad 9.3.5$$

$$\gamma_{\phi\theta} = -\sin\theta\,(2Ba/3Et)\,[(2+\cos\phi)(1-\cos\phi)(1+\upsilon)/((1+\cos\phi)\sin\phi)] \qquad 9.3.6$$

The governing differential equations for the displacements are [23]

$$\partial v/\partial\phi + w = a\,\varepsilon_\phi \qquad 9.3.7$$

$$\partial u/\partial\theta + v\cos\phi + w\sin\phi = a\,\varepsilon_\theta \sin\phi \qquad 9.3.8$$

$$(\partial u/\partial\phi)\sin\phi - u\cos\phi + \partial v/\partial\theta = a\,\gamma_{\phi\theta}\sin\phi \qquad 9.3.9$$

Now, the form of the solution can be represented by

$$u=f(\phi)\sin\theta \qquad 9.3.10$$

$$v=g(\phi)\cos\theta \qquad 9.3.11$$

$$w=h(\phi)\cos\theta \qquad 9.3.12$$

where

$$\varepsilon_\phi = \varepsilon_\phi(\phi)\cos\theta \qquad 9.3.13$$

$$\varepsilon_\theta = \varepsilon_\theta(\phi)\ \mathrm{Cos}\ \theta \qquad 9.3.14$$

$$\gamma_{\phi\theta} = \gamma_{\phi\theta}(\phi)\ \mathrm{Sin}\ \theta \qquad 9.3.15$$

Substitution of the assumed form of the solution into equations 9.3.7-9.3.9 produces the following set of differential equations in ϕ.

$$\partial g/\partial\phi + h = a\ \varepsilon_\phi \qquad 9.3.16$$

$$f + g\ \mathrm{Cos}\ \phi + h\ \mathrm{Sin}\ \phi = a\ \varepsilon_\theta\ \mathrm{Sin}\ \phi \qquad 9.3.17$$

$$(\partial f/\partial\phi)\ \mathrm{Sin}\ \phi - f\ \mathrm{Cos}\ \phi - g = a\ \gamma_{\phi\theta}\ \mathrm{Sin}\ \phi \qquad 9.3.18$$

After considerable manipulation of this set of first order differential equations, the following second order differential equation in g is obtained.

$$\partial^2 g/\partial\phi^2 - (\partial g/\partial\phi)\ \mathrm{Cot}\ \phi = a(\gamma_{\phi\theta}/\mathrm{Sin}\ \phi + (\partial\varepsilon_\phi/\partial\phi) - (\partial\varepsilon_\theta/\partial\phi)) \qquad 9.3.19$$

Now, substituting the equations for the strains into 9.3.19, the equation can be solved by reducing it to a first order equation and integrating it from 0 to ϕ. This gives

$$\partial g/\partial\phi = -(Ba^2(1+\upsilon)/3Et)\ \mathrm{Sin}\ \phi\ [\ \mathrm{Log}\ (2/(1+\mathrm{Cos}\ \phi)) - (1/4)\ \mathrm{Sin}^4\ \phi/(1+\mathrm{Cos}\ \phi)^4] \qquad 9.3.20$$

Finally, integrating from 0 to ϕ, the solution for υ=0.5 is

$$g = -(Ba^2/2Et)\,[\,(-3/10)\cos\phi + (3/4)\,(1-\cos\phi) + \cos\phi \log(1+\cos\phi) - \sin^2\phi/(2(1+\cos\phi)^2)] \qquad 9.3.30$$

Substituting 9.3.30 into equation 9.3.16 and performing algebraic manipulation, we obtain

$$h = -(Ba^2/3Et)\,[-3(-1+\cos\phi)(4.2+(2/10)\cos\phi - 4\log(1+\cos\phi)(1+\cos\phi)]/8\sin\phi \qquad 9.3.31$$

Finally, 9.3.31, 9.3.30, and 9.3.17 give

$$f = -(Ba^2/3Et)\,[36.6-2.4\cos\phi - 27\cos^2\phi - 12\log(1+\cos\phi)(1+\cos\phi)]/8(1+\cos\phi) \qquad 9.3.32$$

Substituting the values of f,g, and h into 9.3.10-9.3.12, the final solution for the non-symmetric displacements on the bladder is obtained.

The plots for these displacements, u,v, and w, are shown in Figures 19-21. These displacements represent the more complex physical behavior of the bladder undergoing non-symmetric loading. However, by noting the values of displacements at certain points, the solutions agree with physical intuition. For example, the meridional displacement v is expected to change sign across the $\theta=\pi/2$ plane (Figure 22). In the non-symmetric loading, the bottom side of the bladder will compress down and the top side will bulge. If two adjacent

points between the unloaded and the loaded state are mapped on the bottom of the shell (Figure 22), the meridional angle change associated with their motion shows a positive increase. This means that meridional displacement, v, should be positive between $\theta=\pi/2$ to $3\pi/2$. This is confirmed by the three dimensional plot. On the top side of the bladder, the opposite effect is seen; the meridional angle change associated with the two points is negative. This indicates a negative meridional displacement from $\theta=3\pi/2$ to $\pi/2$ and is also demonstrated in the graph.

The azimuthal displacement curve can also be examined for physical consistency. Figure 23 demonstrates the type of displacement of the shell parallel circle that occurs during non-symmetric loading. In this case, between 0 and π, the shift in θ between the loaded and unloaded state is positive. Therefore, a positive displacement u is expected. This is demonstrated by the graph in Figure 19. Between π and 2π, the opposite occurs; the azimuthal displacement is negative.

Finally, the displacement from the center of the circle formed by the meridian demonstrates the actual top surface behavior of the bladder under non-symmetric loading. From Figure 21, it is apparent that the top side of the bladder is loaded more than the bottom side. This results in an unbalanced displacement normal to the shell between the top and bottom portions. In Figure 24, a spherical plot of the normal displacement of the shell is shown. This plot represents the actual shape of the bladder under non-symmetric loading. From this plot, it is clear that the bladder is loaded non-symmetrically.

9.4 Additional Considerations for MBAD Bladder Design

Another consideration between the bladder and the heart is the relative motion. Figure 25 demonstrates the relative displacement of neighboring points on the bladder and the heart. Before bladder inflation, the two points are directly adjacent. After inflation, the points experience relative motion. The degree of this motion contributes to the shear stress between the two surfaces. As discussed in the previous analysis, shear stress on the myocardium can result in myocardial necrosis and therefore defeat the main purpose of this cardiac assist device.

One variable that can potentially control this relative motion is the design of the bladder. Specifically, by adjusting the thickness of the bladder, it may be possible to produce a bladder that optimally conforms to the myocardial wall during inflation, causing a minimal amount of relative motion between the two points. The axisymmetric equations for strain, 9.1.6 and 9.1.7, are inversely proportional to the bladder thickness. If the bladder thickness, t, is made a function of ϕ, the following equations represent the strains

$$\varepsilon_\phi = f(\phi)\,(N_\phi - \upsilon N_\theta) \qquad 9.4.1$$

$$\varepsilon_\theta = f(\phi)\,(N_\theta - \upsilon N_\phi) \qquad 9.4.2$$

where $f(\phi)=1/Et(\phi)$. Substitution of 9.4.1 and 9.4.2 into the differential equations for displacement, 9.3.7 and 9.3.8, the following differential equation for v is determined

$$\partial v/\partial \phi - v \cot \phi = a f(\phi) (\varepsilon_\phi - \varepsilon_\theta) \qquad 9.4.3$$

Now, by varying $f(\phi)$, the meridional displacement v is altered. At this stage, the determination of an appropriate $f(\phi)$ seems quite empiric. However, by using various myocardial dimension tracking techniques, such as ultrasonic crystals, perhaps a more thorough knowledge of the actual mechanical properties of the myocardium will be determined. In this case, the meridional displacement of the myocardium could be substituted into equation 9.4.3 and $f(\phi)$ determined. This would assure highly accurate, point-wise matching between the two surfaces.

Unfortunately, the field of cardiac mechanics is severely underdeveloped and this approach is not practical at the present time. However, various hypothetical forms for $f(\phi)$ can be incorporated into the production of the MBAD in a more sophisticated coating process, perhaps involving some form of gas deposition. The effect of this on the relative motion between points on the bladder and heart can be quantified by using an accurate method of myocardial tracking. That is, by stopping the heart, suturing ultrasonic crystals to adjacent points between the bladder and the heart, data regarding relative motion could be obtained.

The bladder thickness can also be varied as a function of θ. This of course complicates the analysis, but none the less presents another variable for altering the deformation pattern of the bladder.

10 Potential Research

Innovative ideas for advancement in device design, actuation, and testing will make the MBAD more useful as a circulatory assist tool.

10.1 Design Improvements

Several design improvements of the MBAD could increase its effectiveness as a circulatory assist device. These improvements range from simple alterations in the production process to advanced concepts for re-design.

In order to increase the effectiveness of the device *in vivo* , there is one minor design alteration that should be implemented: the outer shell must be reinforced through multiple polyurethane coatings. This will preserve device distensibility and still allow removal through a large thoracotomy tube. The advantage of the thickened outer shell could enable increased deformation of the ventricles during inflation as opposed to outward displacement of the shell. Thus, the ejection fraction of the heart would increase. During diastole, the negative pressure surrounding the heart would more likely pull the heart toward the shell, not the shell toward the heart. This effect increases rate of diastolic fill and, potentially, myocardial perfusion.

A more advanced idea requiring device redesign evolved from the major issue of the complex physical interaction between the device bladders and the myocardium during contraction. Presently, the device consists of two bladders that supply equal force to both sides of the heart during inflation. This results in significant ventricular compression of an essentially

motionless heart during fibrillation. However, when the heart is dysfunctional it continues to contract, producing a unique pattern of myocardial deformation. Therefore, application of this device to a beating heart could result in significant shear stress on the epicardium, causing myocardial necrosis.

Accordingly, a method for improving the geometric alignment between the inflating bladder and the deforming ventricle during systole has been devised. This method assumes that a thorough knowledge of the viscoelastic properties of the myocardium are available. It involves dividing each of the two bladders of the device into several smaller bladders,each individually pressure controlled. Piezoelectric crystals could be incorporated into the inner membrane of each bladder to sense the relationship between bladder pressure force and displacement of the myocardium. The analog signal from the piezoelectric crystals could be used as feedback to adjust the amount of pressure filling each bladder. Tuning of the pressure controller would rely on knowledge of myocardial viscoelastic parameters, such as compliance. Thus, the several bladders together would be environmentally sensitive and could apply various amounts of contractile force to each side of the heart at different times during the cardiac cycle. This would result in a much more physiologic deformation during contraction, since the heart communicates with the bladder through its mechanical composition and its dynamic behavior. For example, the midsection of the myocardium thickens the most and contracts with the greatest force during systole. By sending this information to the pressure controller through the piezoelectric signal, the corresponding bladder could be inflated to apply more or less force in this area.

This method would require a controller that was precisely tuned to the viscoelastic properties of the heart. Also, the delivery of air to and from the individual bladders would need to be extremely rapid.

The replication of the natural heart is an area of improvement in device production that has also been postulated. This method would require utilizing the highly accurate diagnostic technique known as magnetic resonance imaging (MRI). MRI images of an intact heart could be obtained in many two-dimensional slices. These slices could then be converted to a three-dimensional image utilizing three-dimensional modelling software. This data could then be used in a manufacturing process known as stereolithography. This production method involves laser cutting the computerized three-dimensional object into a series of cross sections. Each cross section is then carefully sprayed with a finite amount of atomized material, such as metal or plastic. Then they are stacked, and the spraying process is repeated. The end result is a solid, three-dimensional object requiring no machining.

The advantage of this heart replication process is that the device could be custom made to fit a given heart. Also, the time-consuming molding process would be completely eliminated. Finally, if plastic was used as the spraying material, coating the mold would be unnecessary.

10.2 Device Actuation Advancements

The major area for improvement in device actuation is the rate of delivery of air to and from the bladders. This must be accomplished extremely rapidly in order to preserve the true physiologic patterns of myocardial contraction. Presently, the portable power unit supplies ample

volume of air to the bladders at a reasonably fast rate. By increasing the volume output of the IABP console, a more rapid supply of air to and from the bladders could be obtained.

10.3 Future Testing Protocol

An important determinant of the eventual clinical use of the MBAD is a solid testing process. Potential bench and animal testing protocols for the MBAD have been developed. Specifically, a modified Penn State mock circulatory loop would reveal the hydraulic performance of the device. This bench test would model physiologic parameters of the circulatory system such as compliance, systemic vascular resistance, and atrial preload (Figure 26). The Penn State compliance chambers consist of rolling diaphragm piston chambers compressed by a cantilever spring. The Penn State simulated vascular resistance is a flow dividing compression plate. The density and viscosity of blood could be simulated with a mixture of saline and glycerol. Finally, atrial preload can be approximated with a fluid column.

By adjusting the compliance chambers, the mock loop resistance, and the atrial preload, the performance of the MBAD can be tested over a wide range of operating conditions. These include various bladder pressures, pump rates, and systemic vascular resistances. Pressure and flow measurement could be used to assess the performance of the device. This test should be performed using a fresh, excised heart to more closely simulate *in vivo* function, as the heart muscle's viscoelastic properties change as it dies.

An animal experiment that measures cardiac output, myocardial deformation, and systemic pressure and flow with and without the MBAD

would supply necessary in vivo information. This could be accomplished by following the two previously defined protocol.

11 Conclusion

A device for cardiac assist using direct ventricular compression has been designed and tested. The device's simplicity of operation and ease of application allow rapid, low-risk use when compared with other forms of circulatory assist.

In the primary animal experiment, the device's successful *in vivo* application was highly dependent on a refined production process and innovations in both design and actuation. Specifically, the male and female molding materials were changed from silicone caulking and plaster to mycrocrystalline wax and plastic resin; this insured that the required accuracy of replicating the geometry of the heart with the device was attained. Also, advancements in the production process reduced manufacturing time and complexity. The incorporation of an increased device length and an elastic band in the extended portion of the device produced a secure fit and a vacuum seal that assisted the diastolic phase of the cardiac cycle. Additionally, the use of compressed air as opposed to dichlorofluoromethane eliminated the environmental and clinical risk of device leak. Finally, through active evacuation of the device bladders by negative pressure, the normal diastolic filling pattern of the heart was augmented and the prevention of the deleterious condition of cardiac tamponade was achieved.

Extensive bench testing has quantitatively demonstrated that the device is not only capable of supplying the necessary compressive force for substantial cardiac ejection, but also possesses the mechanical integrity for long term use. The primary *in vivo* experiment has clearly shown qualitatively that the device produces adequate assist to a fibrillating heart.

The need for a quantitative method for *in vivo* evaluation of the device was met through the development of a myocardial deformation tracking experiment, utilizing ultrasound as a diagnostic tool. The effects of device application have been carefully explored and related to this testing procedure. This method has been verified to supply accurate geometric data for cardiac deformation when compared to other methods in the literature.

An extensive mechanical analysis of the interaction between the device's bladder and the myocardial wall during bladder inflation has been performed; this employed the application of shell theory to the MBAD bladder. The results of this analysis predict bladder wall stress, strain, and displacement under various models of cardiac loading. Specific numeric calculations for these stresses, strains, and displacements rely on further information from the field of cardiac mechanics. They demonstrate that through alteration in the device's bladder wall thickness, it may be possible to minimize relative motion between neighboring points on the bladder and the heart wall. Therefore, the possibility of myocardial necrosis or device failure can be minimized. Although theoretical analysis of the relative motion of the points is limited, experimental evaluation of various bladder wall thicknesses can be performed through ultrasonic measurements.

In conclusion, the development of circulatory assist devices is crucial to the improvement of health care. Presently, most NIH funding has been redirected to the development of circulatory assist devices, not the artificial heart. This suggests that devices such as the mechanical biventricular assist device have tremendous potential as life-saving tools.

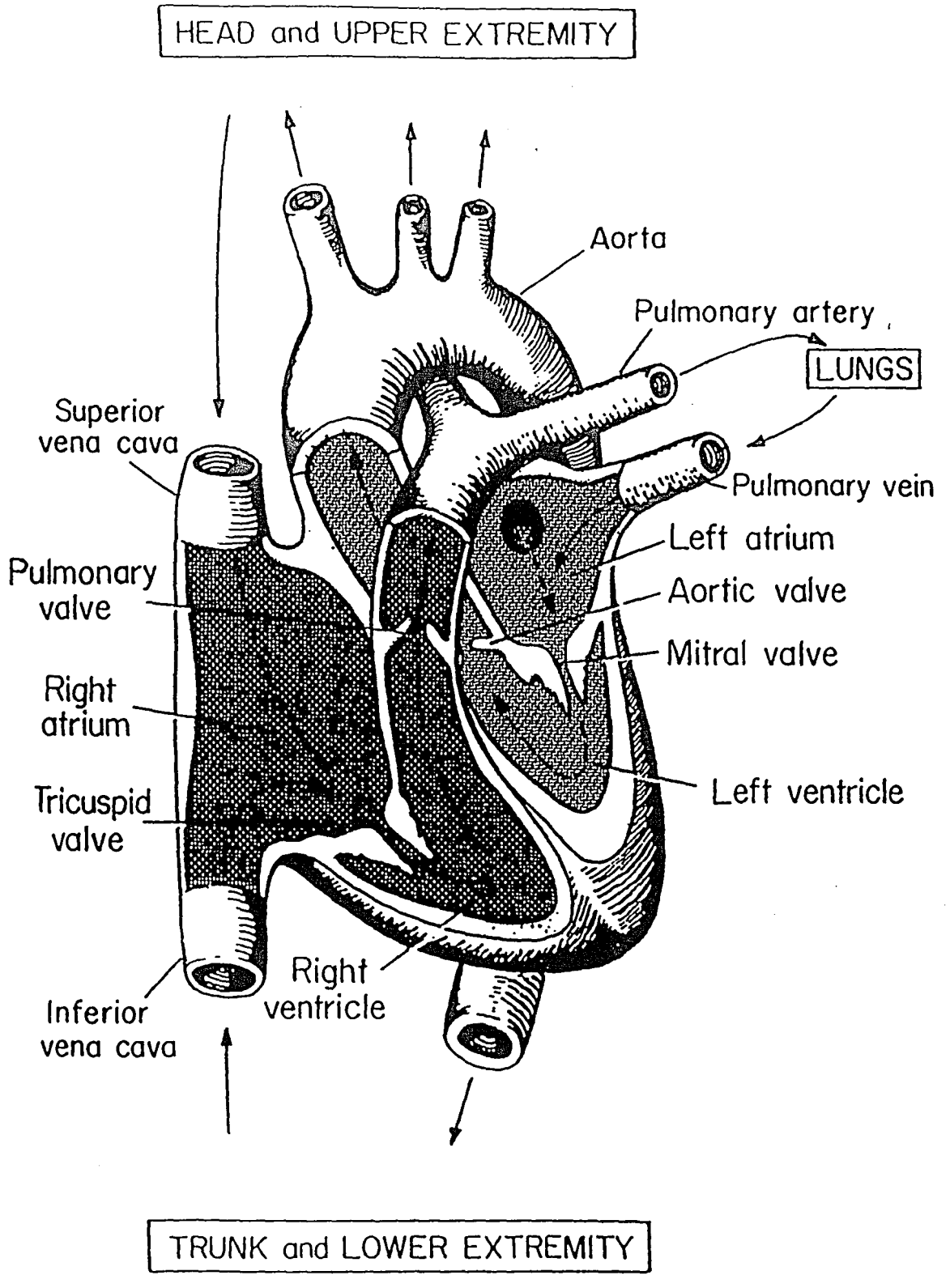

Figure 1: Anatomy and direction of blood flow in the human heart [2].

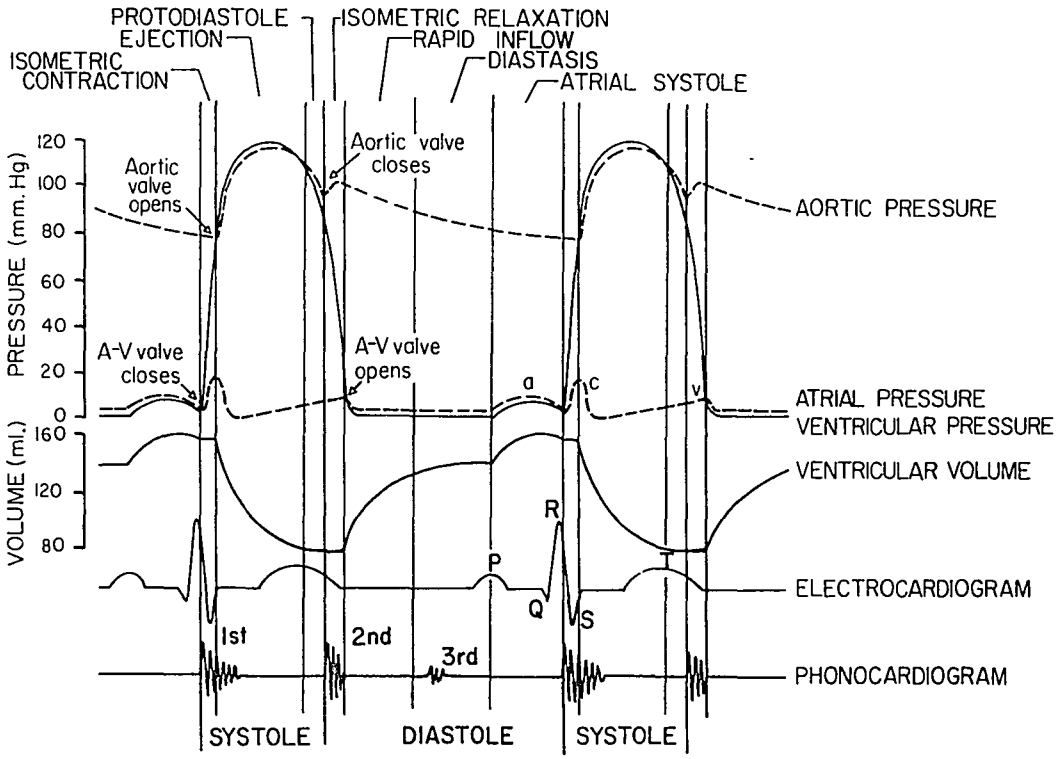

Figure 2: Plot of normal left heart pressure, flow, and volume versus time over two cardiac cycles. ECG and phonocardiogram are included [2].

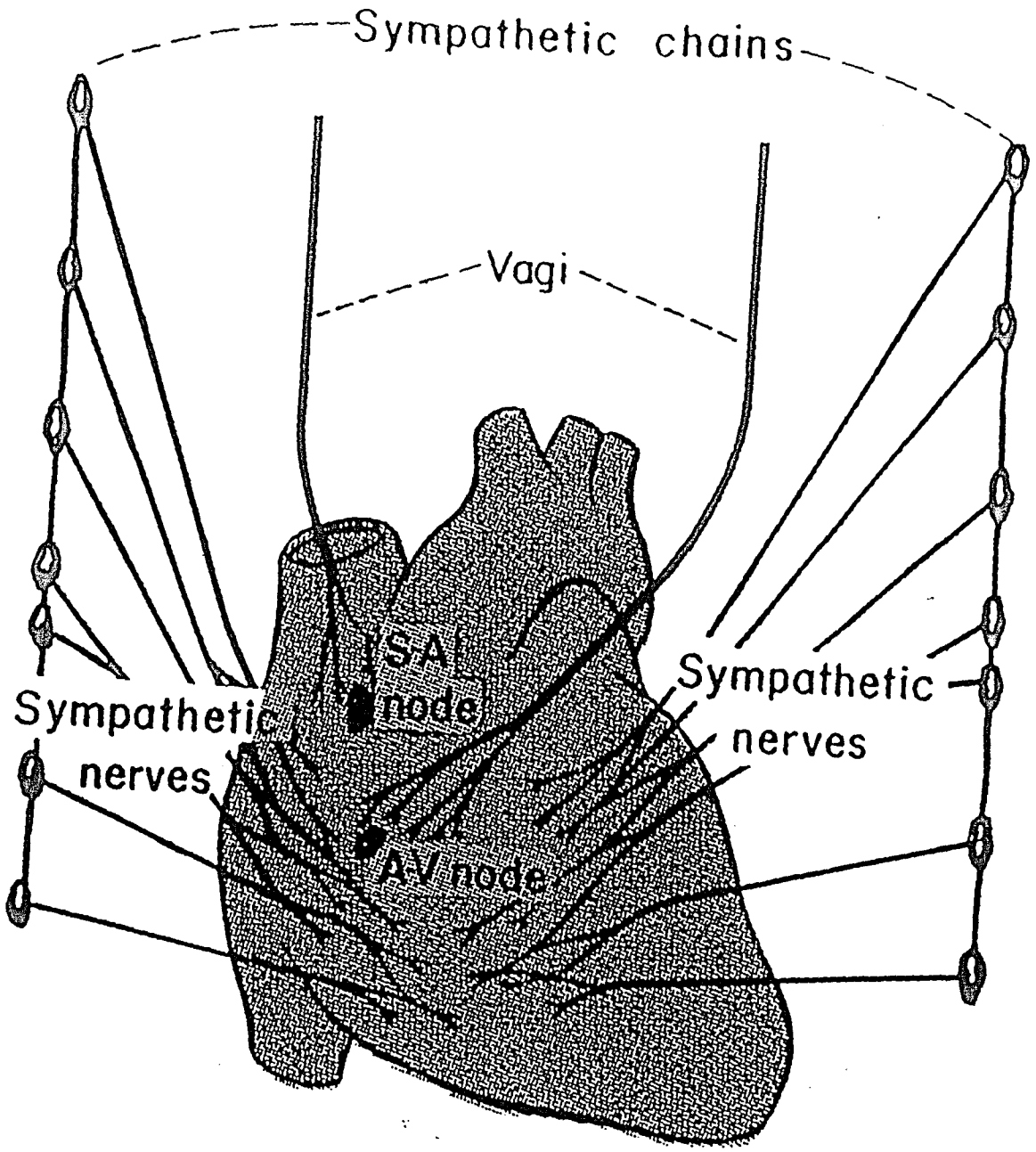

Figure 3: Anatomical location of the sinoatrial and atrioventricular nodes [2].

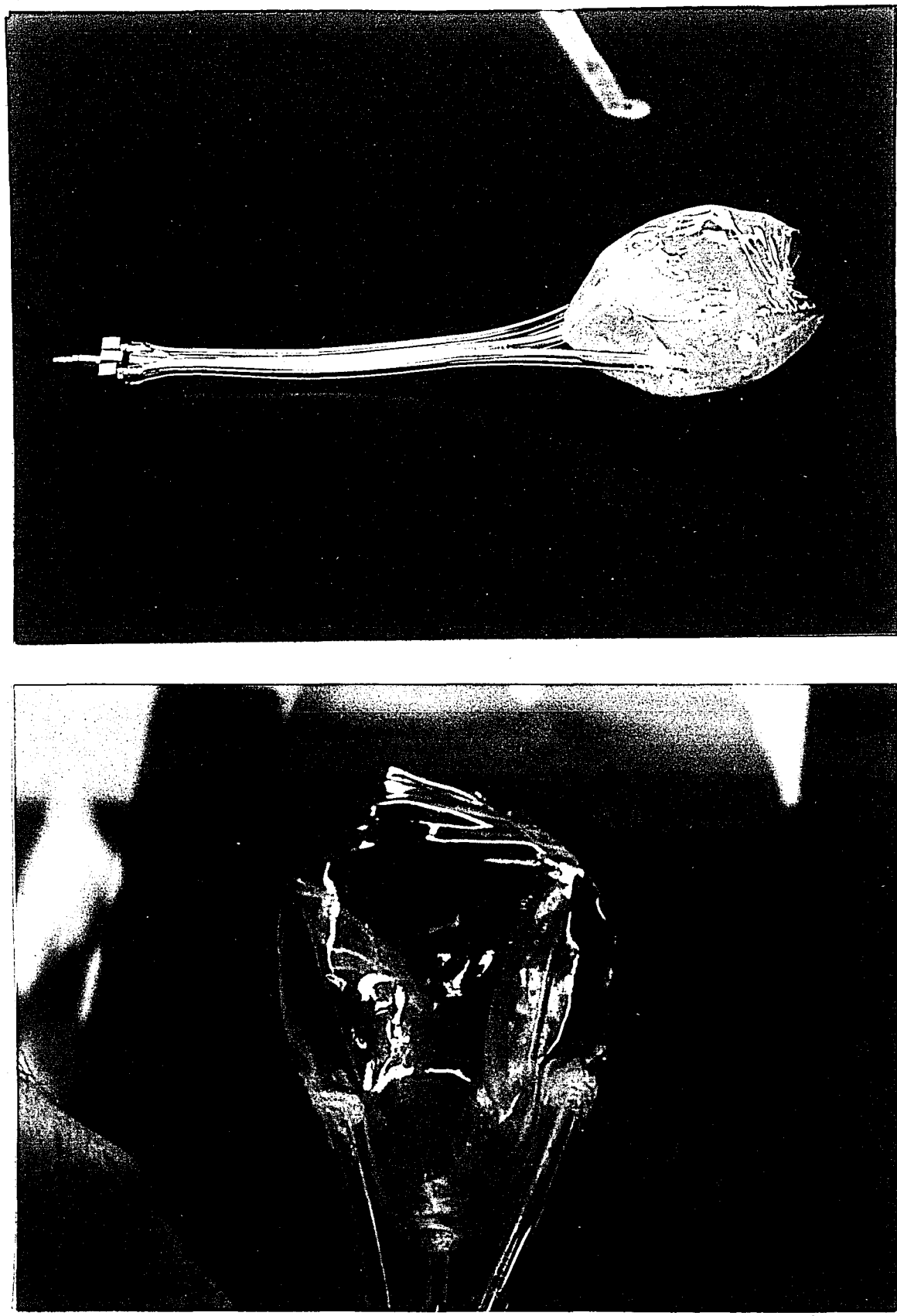

Figure 4: Complete view of the MBAD with tubing and fitting attachments (top). Partial inflation of the device bladders (bottom).

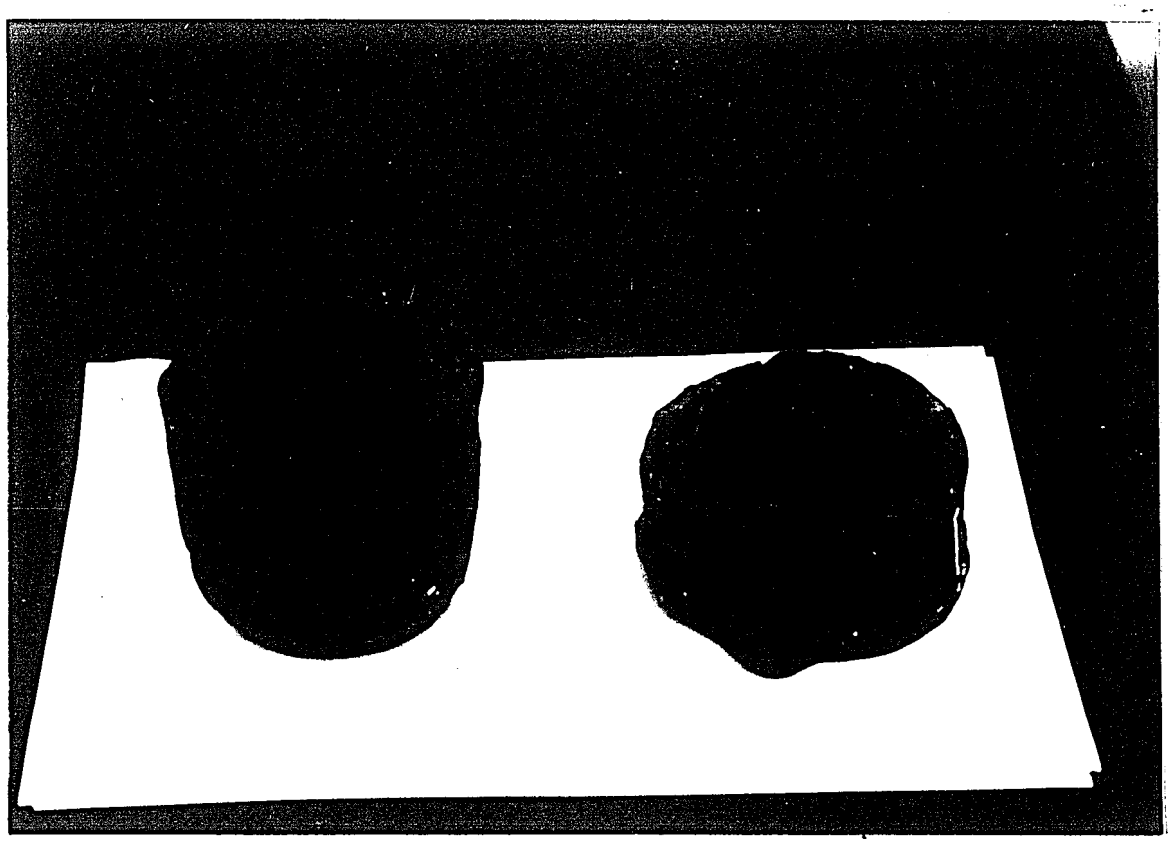

Figure 5: Female microcrystalline wax replica of the heart. Both halves of the mold are shown separated at the seamless parting line.

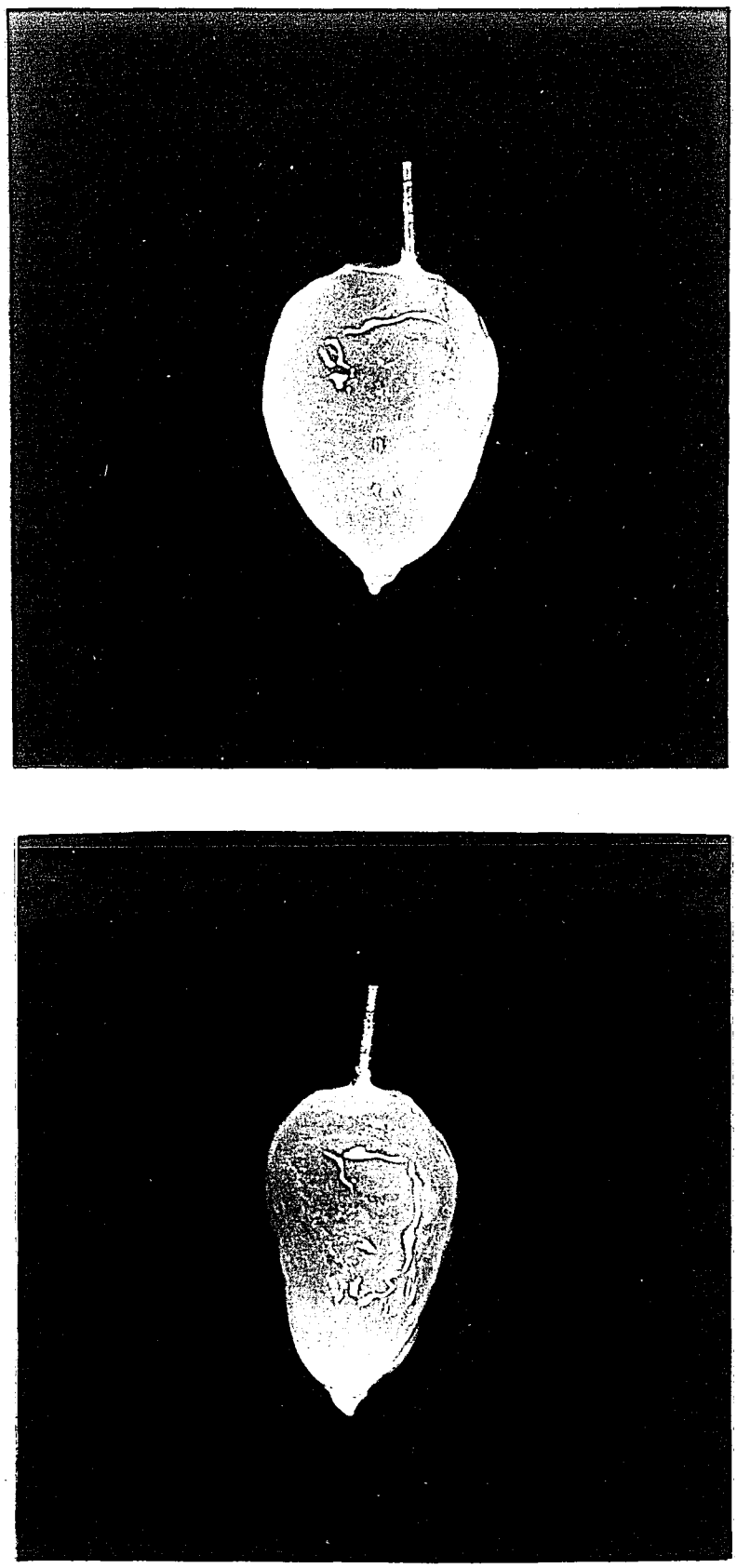

Figure 6: Plastic resin male replica of the natural heart. Frontal view (top). Lateral view (bottom).

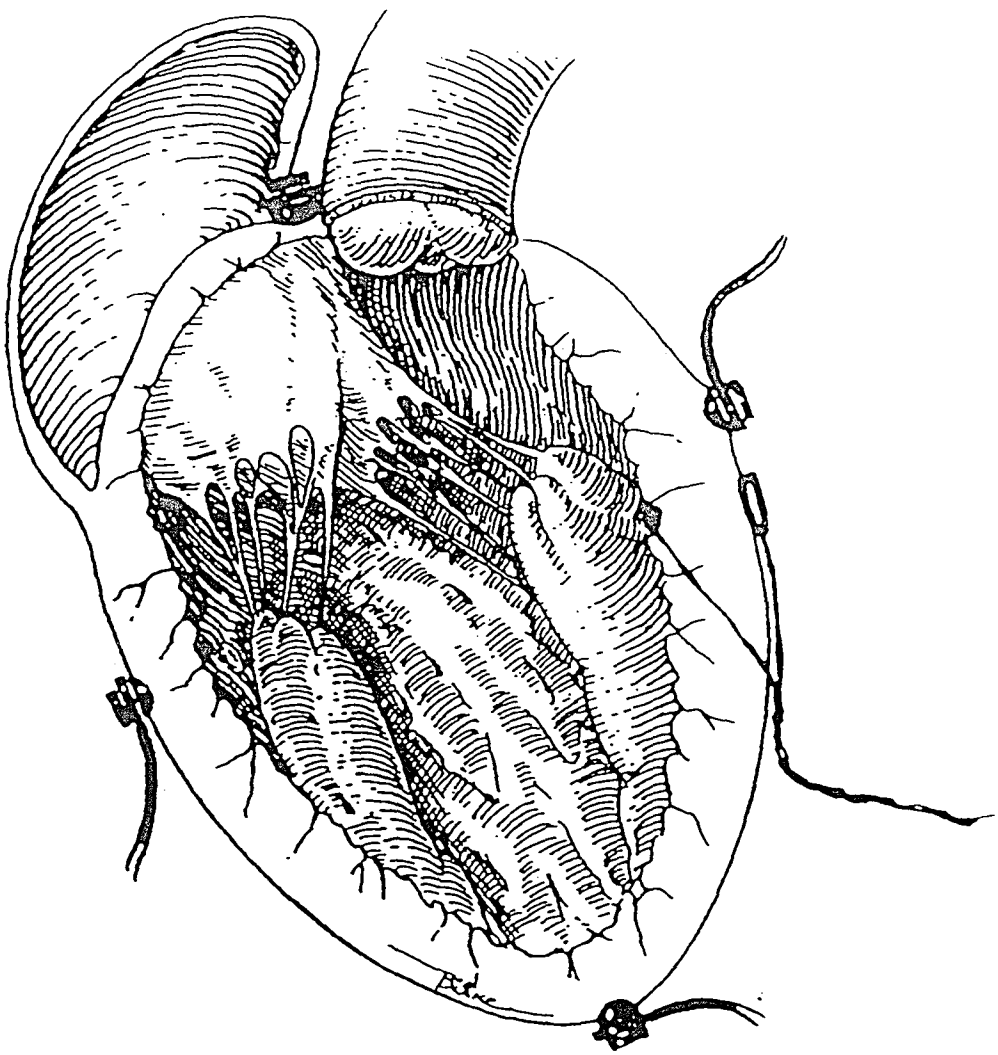

Figure 7: Location of the ultrasonic crystals on the heart for measurement of long axis, short axis, and ventricular wall thickness [22].

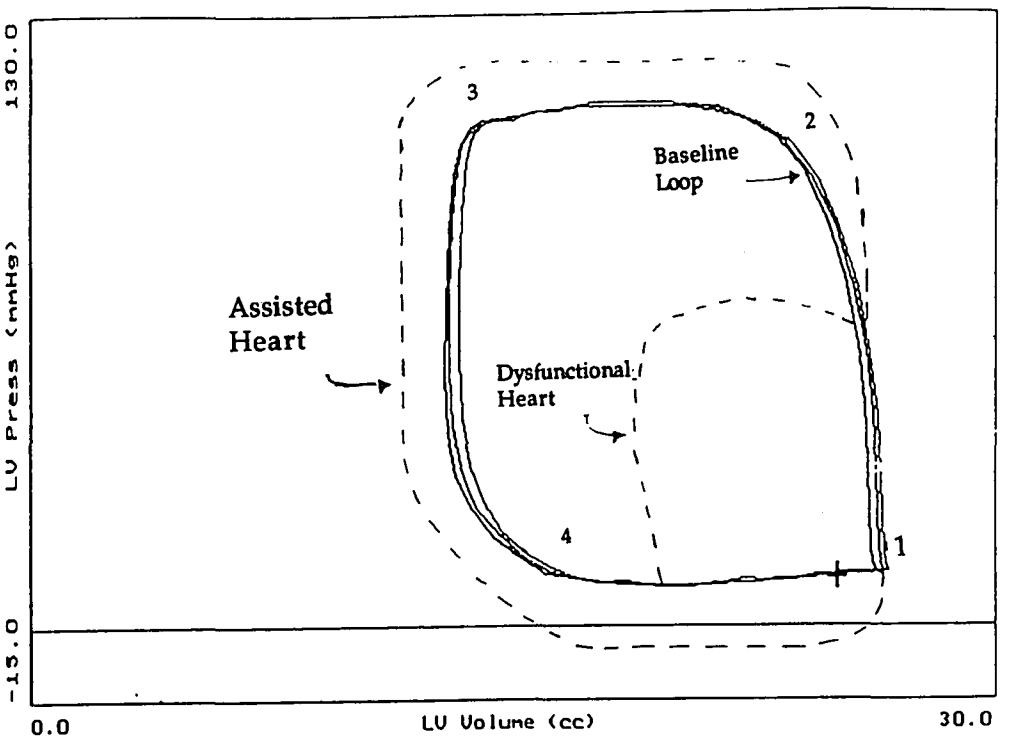

Figure 8: Three baseline pressure-volume loops calculated from the ultrasonic dimension data. The small dotted loop represents the expected behavior of a dysfunctional heart. The larger dotted loop demonstrates the effect of MBAD augmentation.

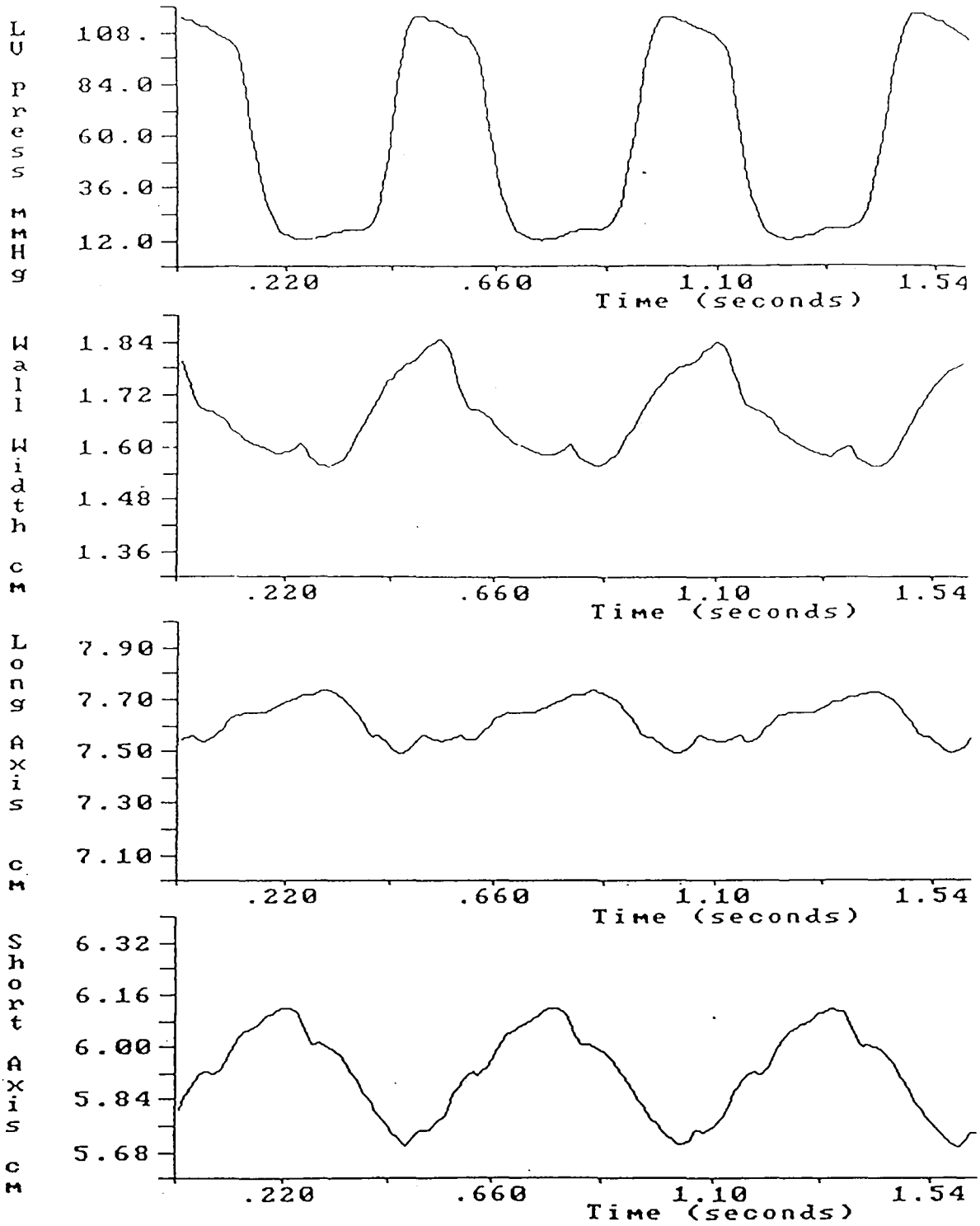

Figure 9: Plot of long axis, short axis, and wall thickness of the heart versus time over three complete cardiac cycles. Left ventricular pressure is plotted in order to associate dimension changes with physiologic events. Note shortening of the long and short axis and thickening of the wall during contraction.

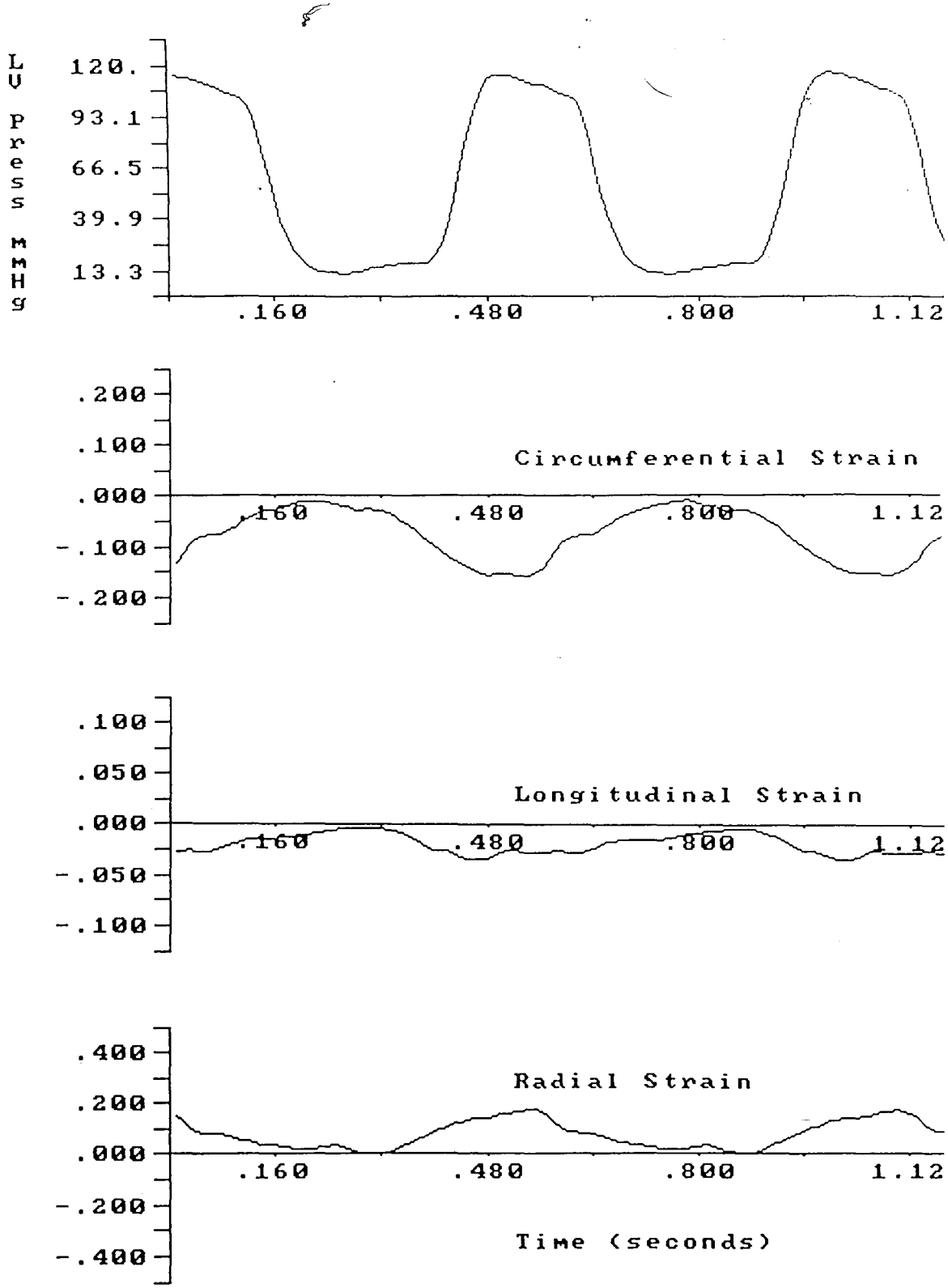

Figure 10: Plot of circumferential, longitudinal, and radial strain of the heart versus time over three complete cardiac cycles. Left ventricular pressure is plotted in order to associate strain variation with physiologic events. Note substantial radial and circumferential strain.

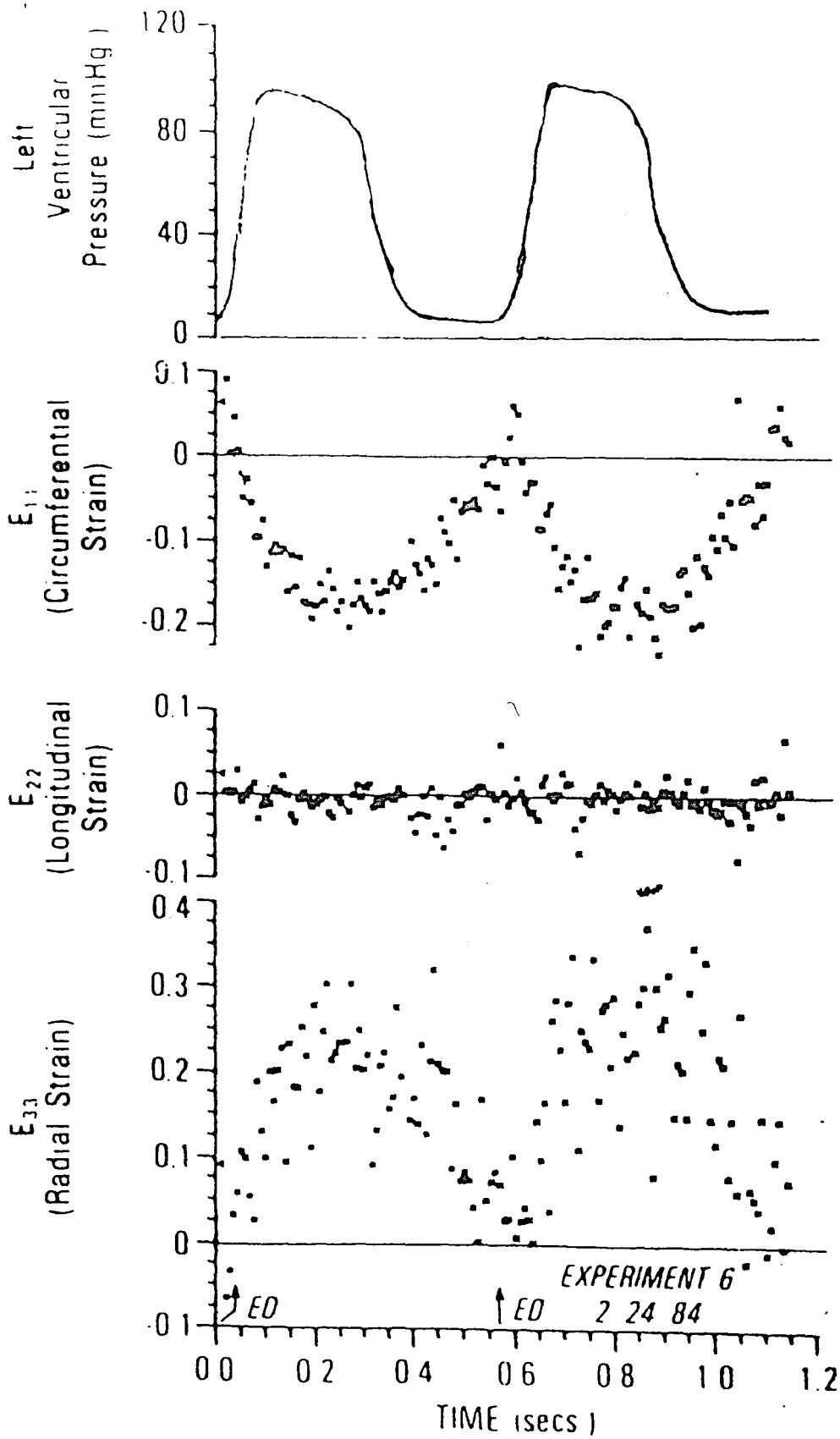

Figure 11: Plot of circumferential, longitudinal, and radial strain of the heart versus time over two complete cardiac cycles from Waldman [20].

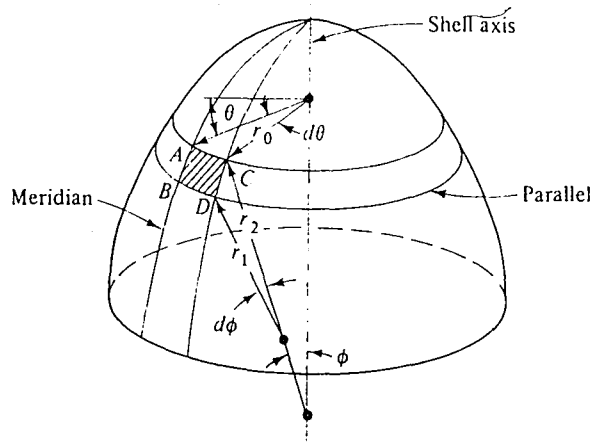

Figure 12: Spherical shell representation of the MBAD bladder [24]. The shell surface is formed by rotating the meridian about the shell axis. The meridional angle, ϕ, is measured down from the shell axis. The azimuthal angle, θ, is measured around the shell axis.

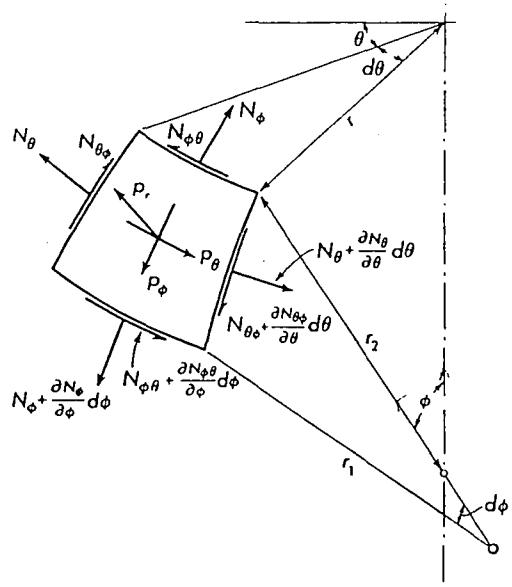

Figure 13: Shell element showing pressure loading and stress resultants [23].

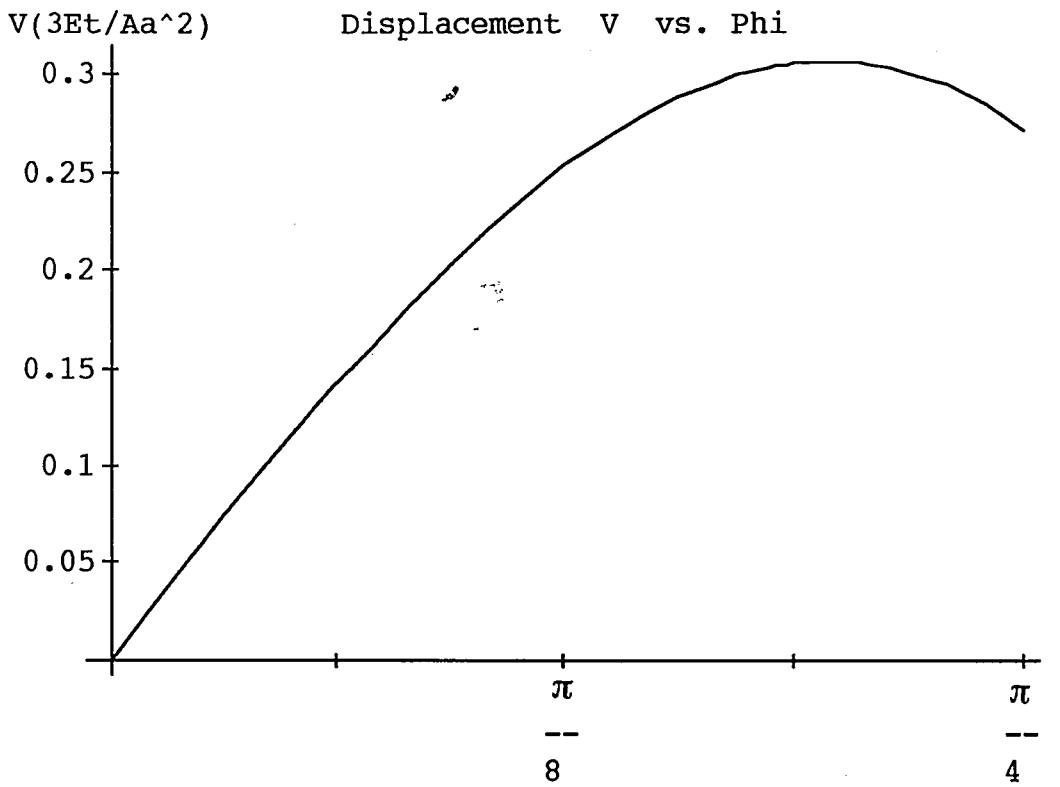

Figure 14: Meridional displacement v versus ϕ for axisymmetric pressure loading. v is multiplied by $3Et/Aa^2$ to obtain a normalized plot.

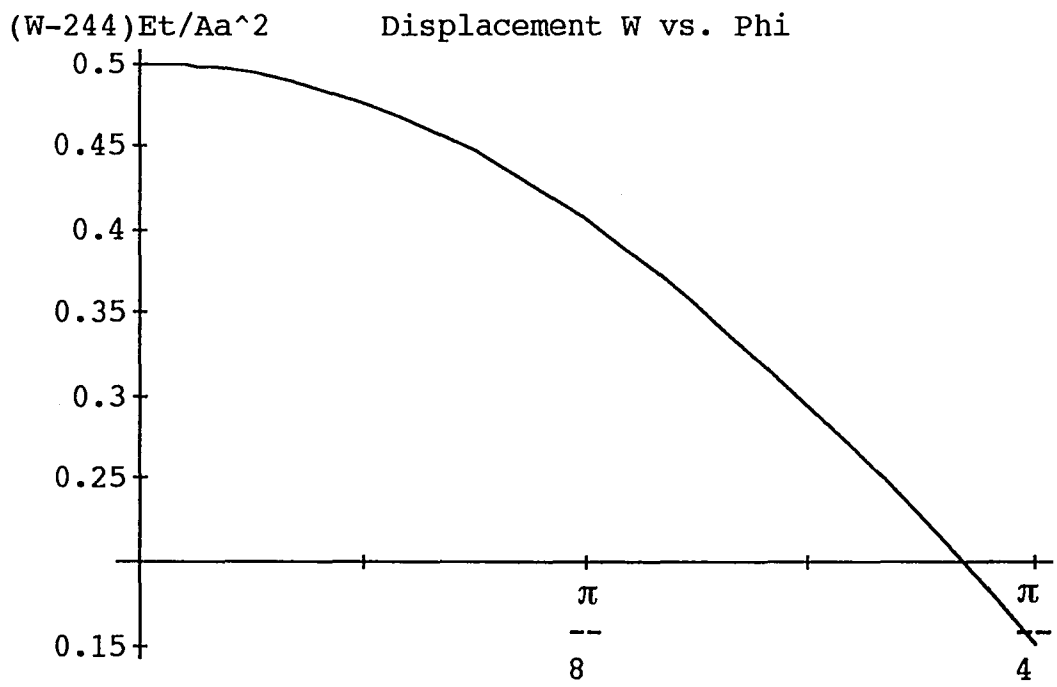

Figure 15: Normal displacement w versus ϕ for axisymmetric pressure loading. The plot is normalized by subtracting $(1/4)\, P_o\, a^2/Et$ from w and multiplying by Et/Aa^2, where P_o=3psi (2.1×10^4 N/m^2), E=1.6psi (1.1×10^4 N/m^2), a=2.5 in (6.35 cm), and t=0.012 in (0.03 cm).

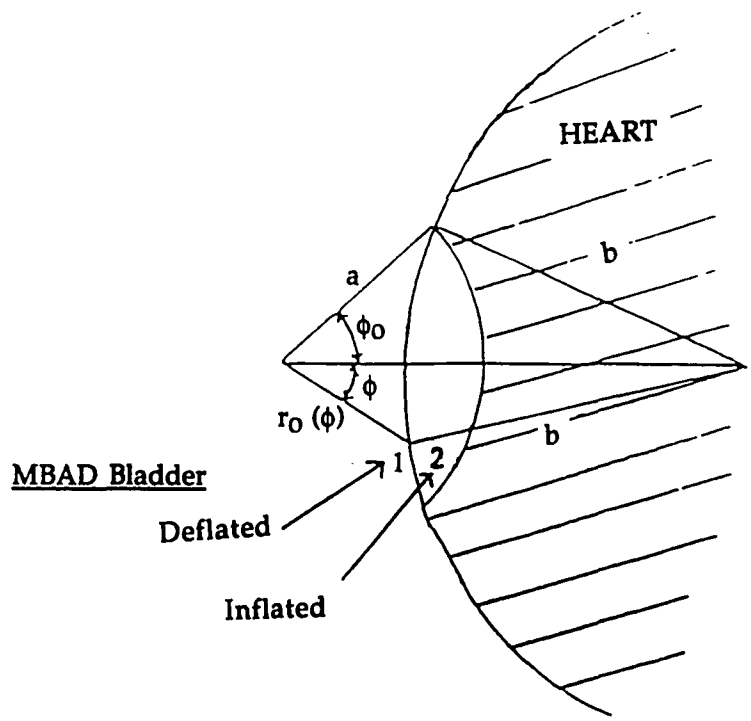

Figure 16: Geometric relationship between the MBAD bladder surface and the myocardial surface. Bladder position 1 occurs during deflation and position 2 during inflation.

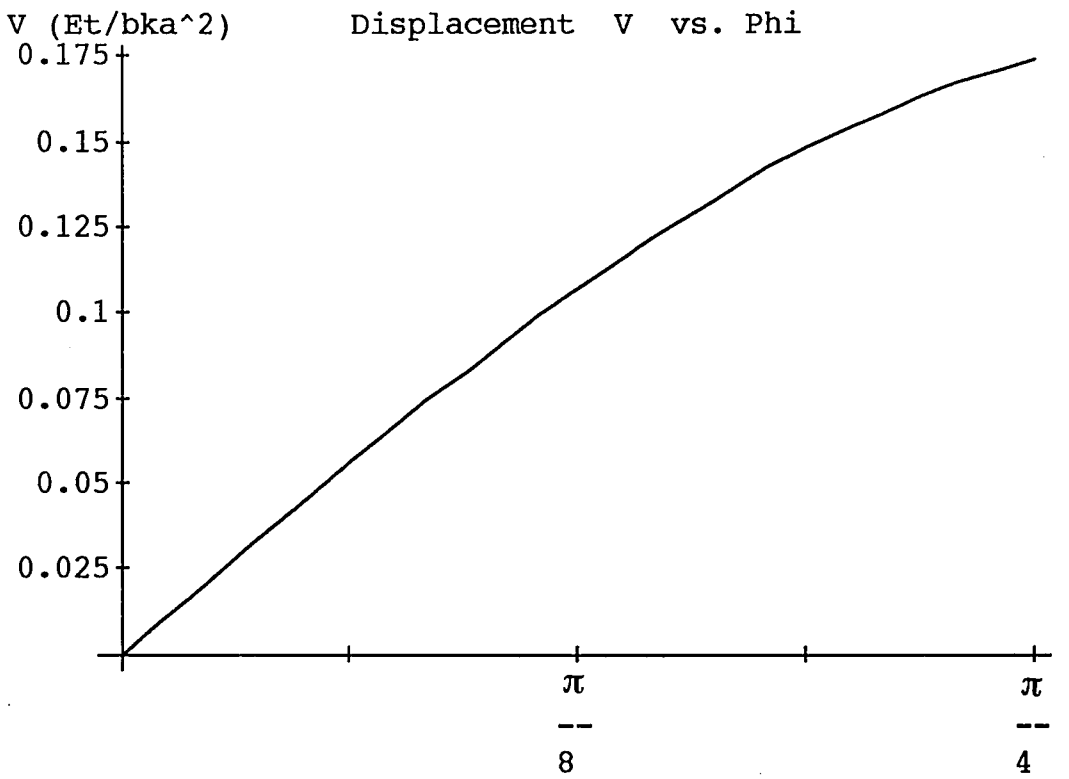

Figure 17: Meridional displacement v versus ϕ for axisymmetric pressure loading. v is multiplied by Et/bka^2 to obtain a normalized plot.

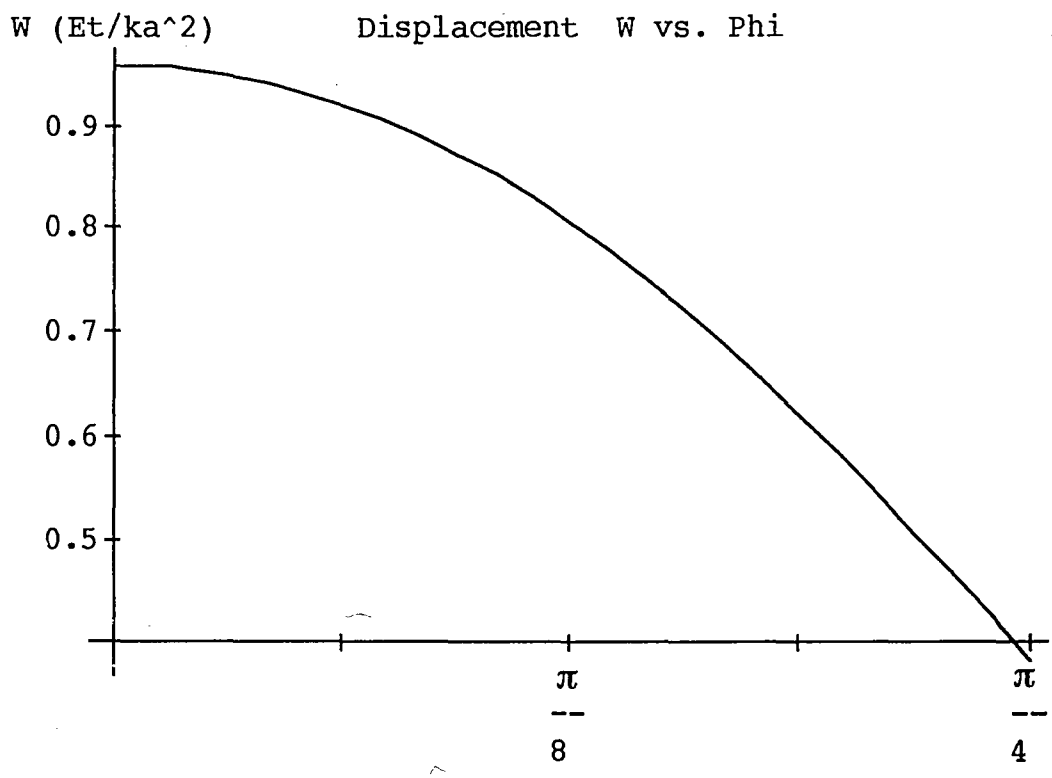

Figure 18: Normal displacement w versus ϕ for axisymmetric pressure loading. The plot is normalized by multiplying w with Et/ka^2.

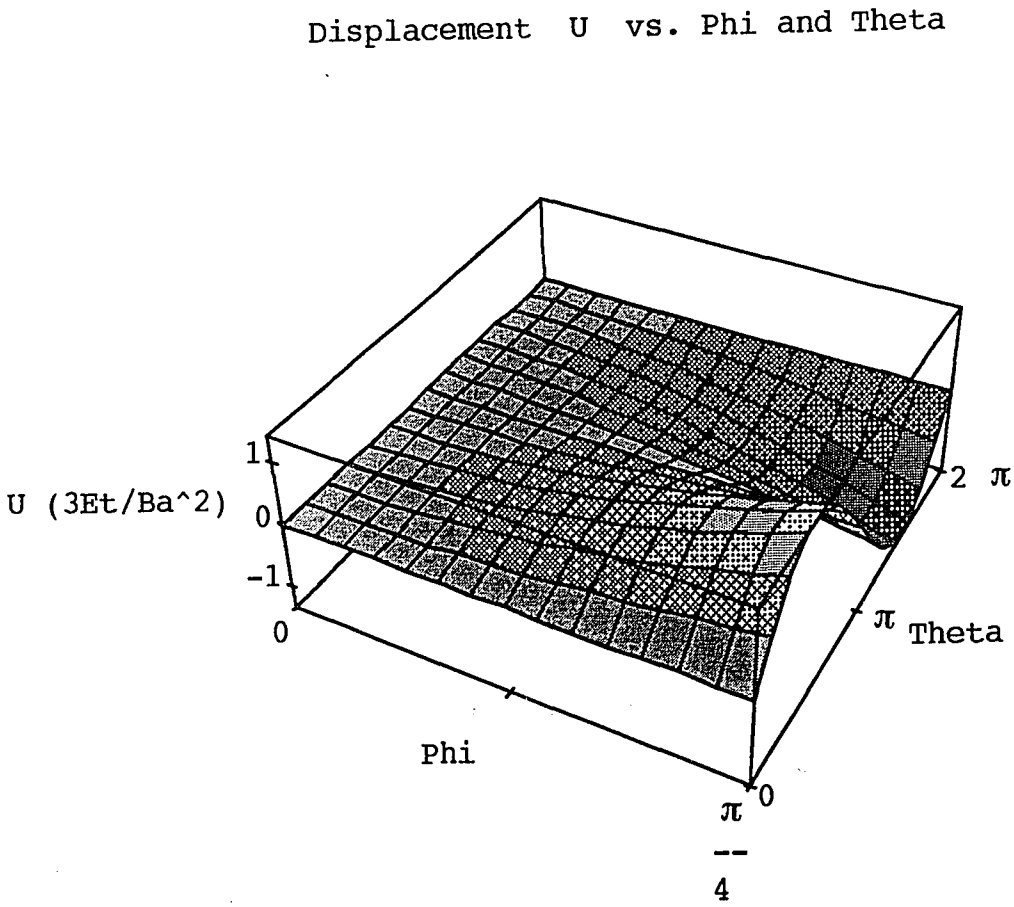

Figure 19: Azimuthal displacement u versus ϕ and θ for non-symmetric pressure loading. u is normalized by multiplying with $3Et/Ba^2$.

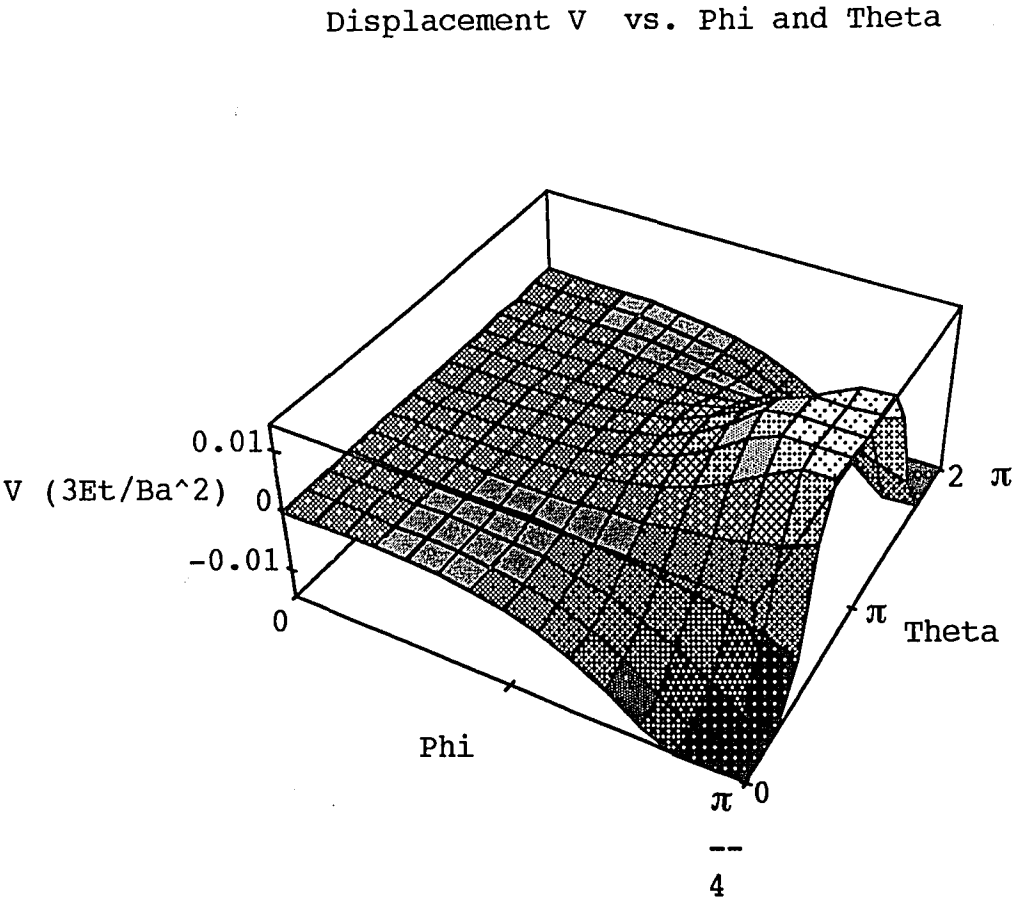

Figure 20: Meridional displacement v versus ϕ and θ for non-symmetric pressure loading. v is normalized by multiplying with $3Et/Ba^2$.

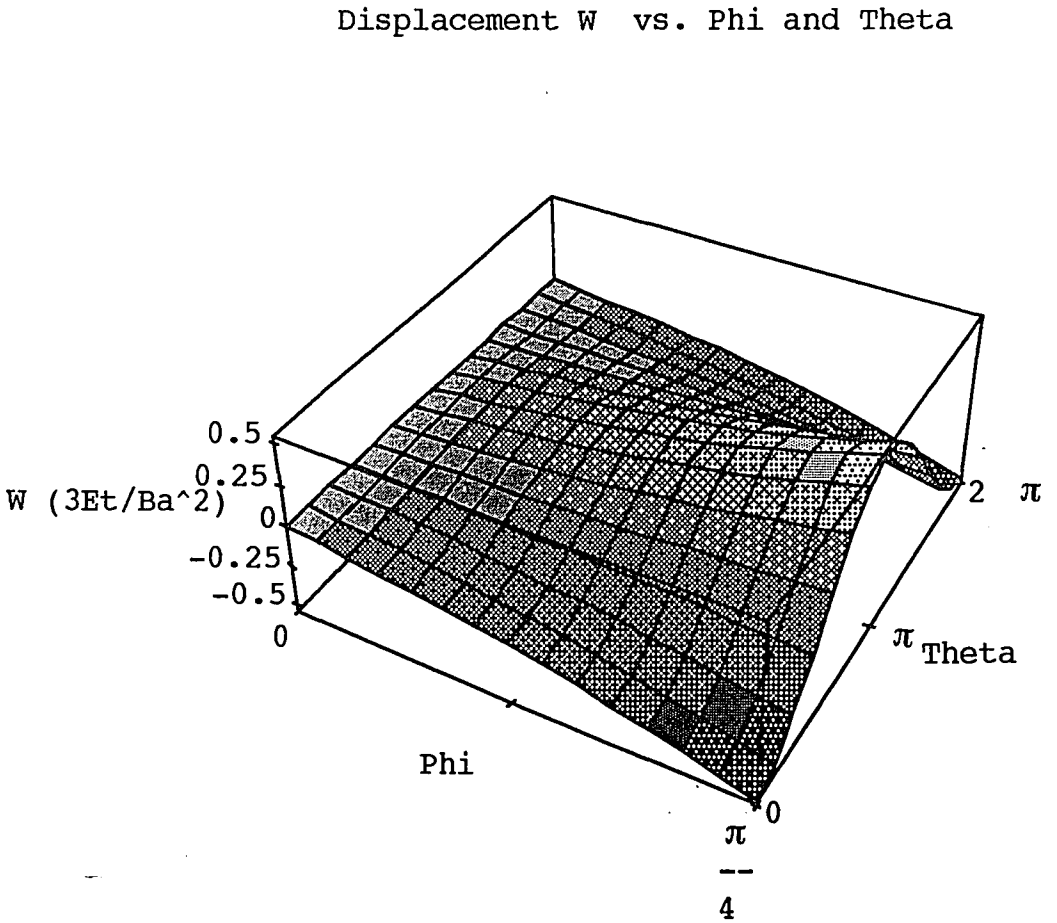

Figure 21: Normal displacement w versus ϕ and θ for non-symmetric pressure loading. w is normalized by multiplying with $3Et/Ba^2$.

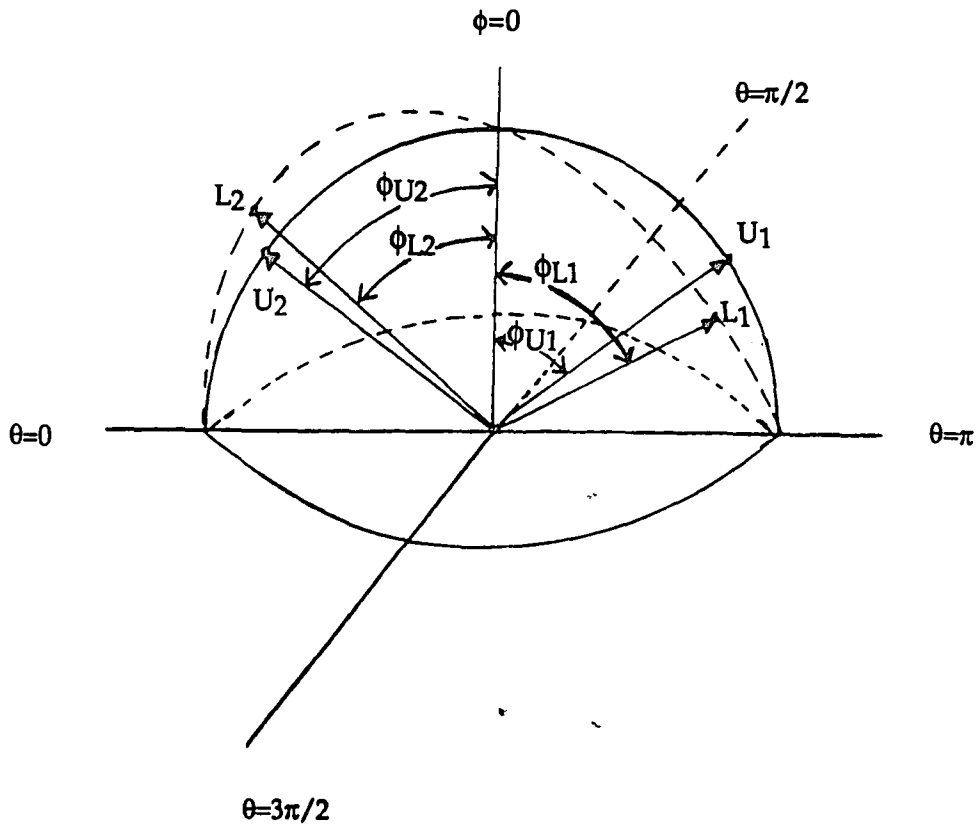

Figure 22: The effect of non-symmetric pressure loading on the meridional displacement. U_1 and U_2 represent the location of two points on the unloaded bladder. L_1 and L_2 are the same points on the bladder in the loaded configuration. From $\theta=\pi/2$ to $3\pi/2$, the angle change associated with the meridional displacement of these points is positive, therefore the displacement is positive. The opposite occurs on the other side of the $\theta=\pi/2$ plane, where the displacement is negative.

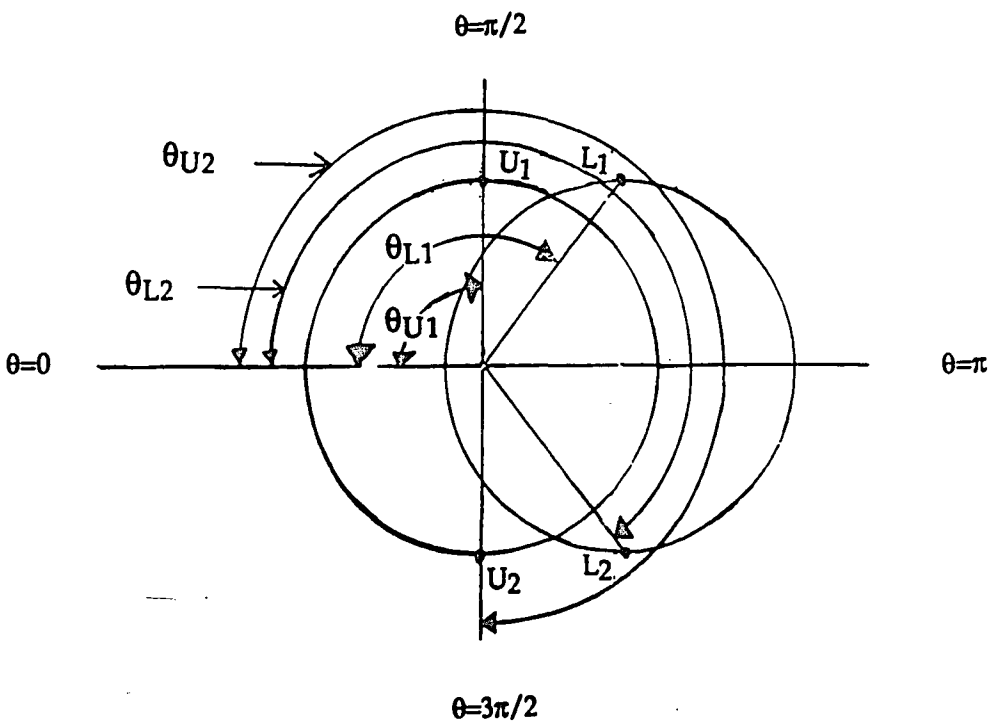

Figure 23: The effect of non-symmetric pressure loading on the azimuthal displacement. U_1 and U_2 represent the location of two points on the parallel circle of the unloaded bladder. L_1 and L_2 are the same points on the bladder in the loaded configuration, where the parallel circle shifts. From $\theta=0$ to π, the angle change associated with the azimuthal displacement of these points is positive, therefore the displacement is positive. The opposite occurs on the other side of the $\theta=\pi$ plane, where the displacement is negative.

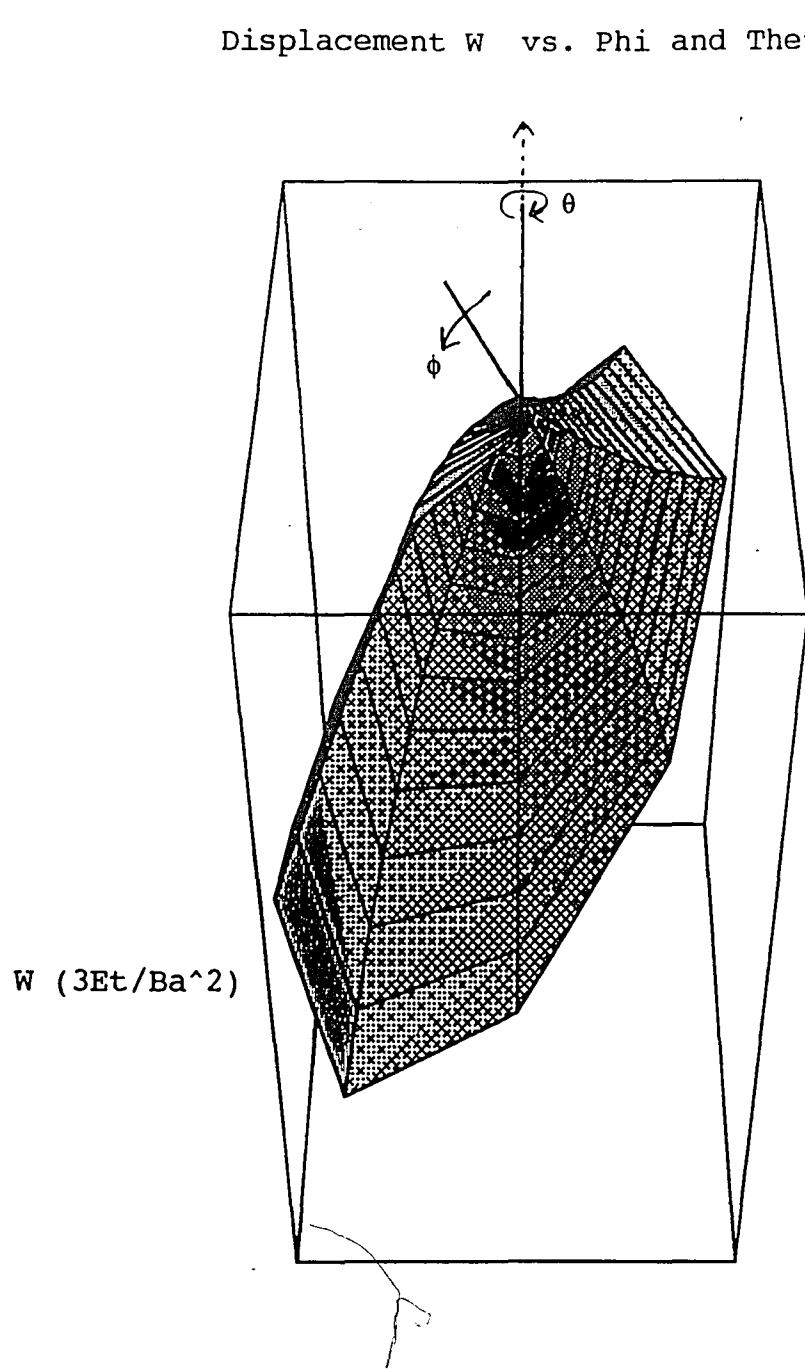

Figure 24: Spherical plot of the normal displacement of the shell under non-symmetric loading. This surface represents the actual shape of the MBAD bladder. θ is measured around the shell axis and ϕ down from the shell axis.

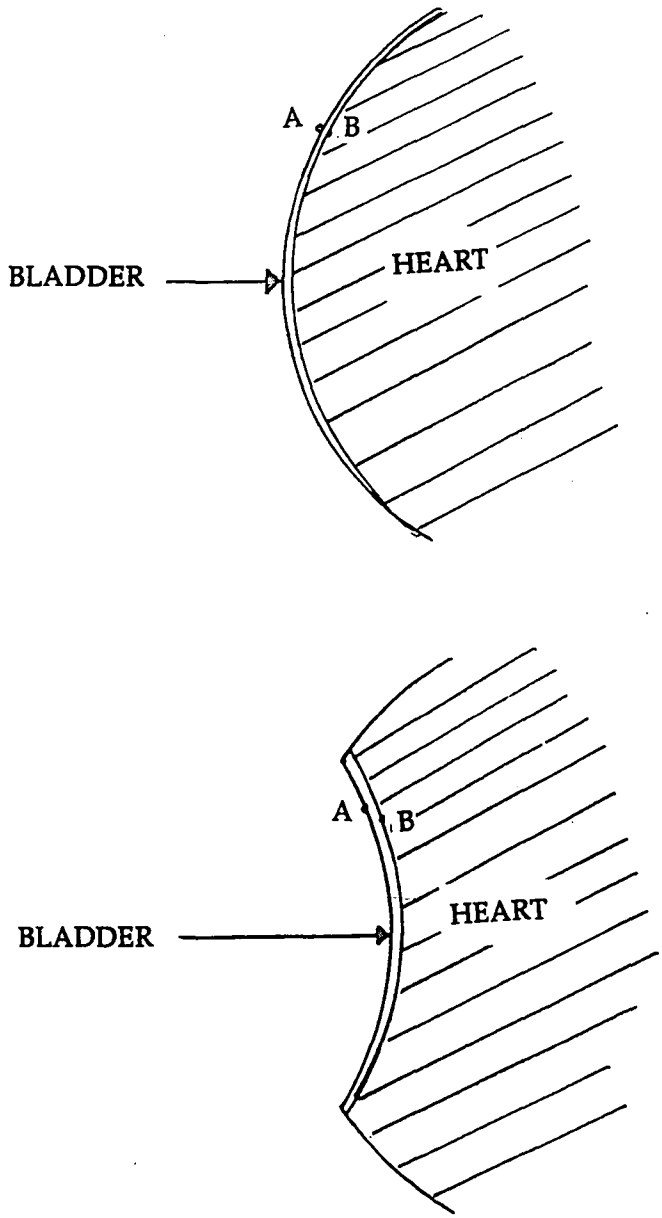

Figure 25: Upper figure: Location of two adjacent points, A and B, on the bladder and the myocardium before bladder inflation. Lower figure: Relative displacement of the two points after bladder inflation.

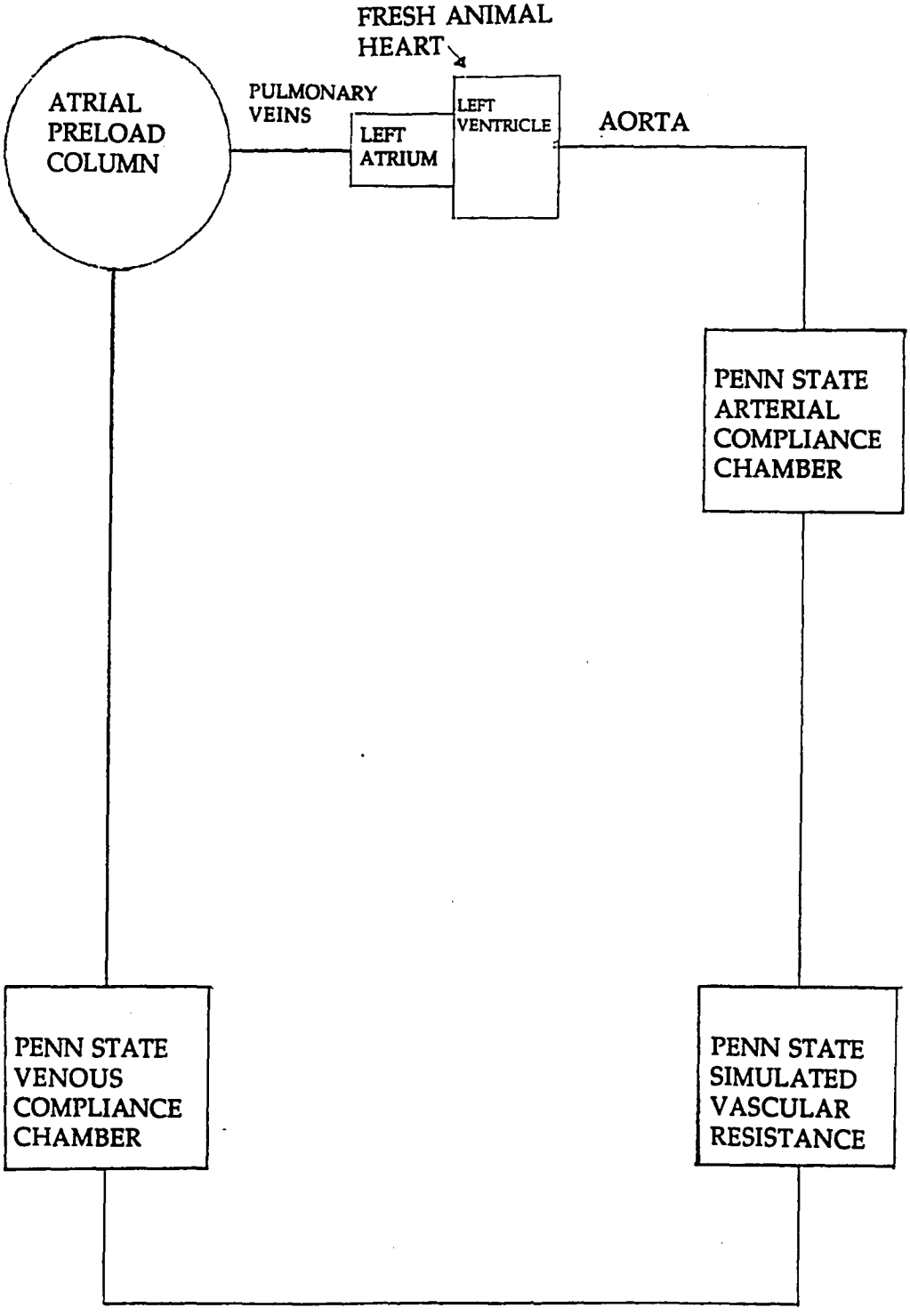

Figure 26: Schematic of a modified Penn State mock circulatory loop for potential use in MBAD bench testing. Physiologic compliance and resistance are simulated with mechanical elements.

References

1. Anstadt, Mark P., "Direct Mechanical Ventricular Actuation: A Review" *Resuscitation*, Vol. 21 (1991), pp. 7-23.

2. Guyton, Arthur C. Textbook of Medical Physiology. 6th ed. Philadelphia: Saunders Co., 1985.

3. Anstadt, George L., "A New Instrument for Prolonged Mechanical Massage", *Circulation*, Vol. 31 (1965), pp. 43-44.

4. Anstadt, George L., "Continued Studies in Prolonged Circulatory Support by Direct Mechanical Assistance", *American Society of Artificial Internal Organs*, Vol. 14 (1968), pp. 297-303.

5. Anstadt, George L., "Prolonged Circulatory Circulatory Support by Direct Mechanical Ventricular Assistance for 2-3 Days of Ventricular Fibrillation", *American Society of Artificial Internal Organs*, Vol. 17 (1971), pp. 174-182.

6. Skinner, David B., "Applications of Mechanical Ventricular Assistance", *Annals of Surgery*, Vol. 166 (1967), pp. 500-512.

7. Anstadt, George L., "Acute Circulatory Support by Mechanical Ventricular Assistance Following Myocardial Infarction", *Journal of Thoracic and Cardiovascular Surgery*, Vol. 54 (1967), pp. 785-806.

8. Skinner, David B., "Mechanical Ventricular Assistance: Applications of a Method for Total Cardiac Support", *Bull. Soc. Int. Chir.*, Vol. 3 (1969), pp. 406-412.

9. McCabe, J.B., "Direct Mechanical Ventricular Assistance During Ventricular Fibrillation", *Annals of Emergency Medicine*, Vol. 12 (1983), pp. 21-26.

10. Bartlett, R. I., "Comparative Study of three Methods of Resuscitation: Closed Chest, Open Chest Manual, and Direct Mechanical Ventricular Assistance", *Annals of Emergency Medicine*, Vol. 13 (1984), pp. 24-28.

11. Brown, C.G., "Effect of Direct Mechanical Ventricular Assitance on Myocardial Hemodynamics During Ventricular Fibrillation", *Critical Care Medicine*, Vol. 17 (1989), pp. 1175-1180.

12. Skinner, David B., "Surgery for Acute Myocardial Infarction: Coronary Flow and Heart Work During Total Circulatory Support", *Surgery*, Vol. 68 (1970), pp. 128-135.

13. Skinner, David B., "Left Circumflex Coronary Artery Division in Dogs Given Supportive Treatment, *Annals of Thoracic Surgery*, Vol. 7 (1969), pp. 242-245.

14. Skinner, David B., "Successful Kidney Transplantation After 6 h of Cadaver Organ Perservation by Mechanical Ventricular Assistance", *Journal of Surgical Research*, Vol. 10 (1987), pp. 287-288.

15. Skinner, David B., "Resuscitation Following Prolonged Cardiac Arrest", *Annals of Thoracic Surgery*", Vol. 11 (1971), pp. 201-209.

16. Veith, F.C., "Lung, Liver, and Kidney Preservation in Transplantation", *Transplantation Proceedings*, Vol. 1 (1969), pp. 808-818.

17. Anstadt, Mark P., "Mechanical Cardiac Actuation Achieves Hemodynamics Similar to Cardiopulmonary Bypass", *Surgery*, Vol. 108 (1990), pp. 442-451.

18. Anstadt, Mark P., " Mechanical Myocardial Actuation During Ventricular Fibrillation Improves Tolerance to Ischemia Compared to Cardiopulmonary Bypass, *Circulation*, (1990) (in Press).

19. Grossman, William J., "Evaluation of Systolic and Diastolic Function of the Myocardium" *Cardiac Catheterization and Angiography*, Vol. 1 (1985), pp. 301-319.

20. Waldman, Lewis K., "Transmural Myocardial Deformation in the Canine Left Ventricle" *Circulation Research,* Vol. 57 (1985), pp. 152-163.

21. Rankin, J. Scott., "Viscoelastic Properties of the Diastolic Left Ventricle in the Conscious Dog" *Circulation Research,* Vol. 41 (1977), pp. 44-56.

22. Rankin, J. Scott., "The Three-Dimensional Dynamic Geometry of the Left Ventricle in the Conscious Dog" *Circulation Research,* Vol. 39 (1976), pp. 37-45.

23. Flugge, Wilhem, Stresses in Shells. 2nd ed., Springer-Verlag, 1973.

24. Ugural, A.C., Stresses in Plates and Shells. McGraw-Hill, 1981.

Appendix A

Steps in the Molding Process

FEMALE MOLD

1. Obtain natural heart from Baringer Brothers.
2. Prepare heart for molding:
    a. remove excess fat
    b. remove major blood vessels as closely to the heart as possible.
    c. fill the ventricles with gauze
    d. seal off the entrances of the vessels with silicone rubber, shaping the material into the heart.
3. Suspend heart in container via nylon string and hook oriented with the apex pointing down.
4. Melt wax in the accompanying aluminum container.
5. Pour first layer of wax up to the widest cross section of the heart.
6. Allow wax to dry and carefully remove the heart from this half of the mold.
7. Wipe the top surface of the wax to roughen it to allow the paint to adhere.
8. Spray 3-4 coats of red high temperature engine enamel on the top surface of the wax and allow to dry 30 minutes between each coat. Allow the several hours to dry after final coat.
9. Re-position the heart in the mold and melt wax again.
10. Pour in small amount of wax and let dry for 1 hour (This

small volume prevents excessive heat transfer between the recently heated wax and the dry wax below the painted surface since it is such a small amount. Also, it serves to insulate the painted parting line from the large volume remaining to be poured).

11. Pour in the remaining wax to completely cover the heart.
12. Allow wax to 1-3 hours.
13. Mark both halves of the mold in order to maintain alignment and carefully pull mold apart to remove heart.

MALE MOLD

1. After female mold is dry, reassemble and align each half of the mold.
2. Cut 1 inch diameter hole in top half to allow opening for the pouring of the molding material.
3. Suspend threaded bolt with nylon string within the bounds of the female mold to create handle for male mold.
4. Place the wax mold in freezer to cool for molding process.
5. Mix plastic resin with the appropriate amount of hardener depending on mold thickness. (More hardener for larger molds).
6. Pour the mixture into the cooled wax mold in several steps, tapping the mold between each to eliminate any potential air.
7. Place container in refrigerator to eliminate wax melting during the exothermic reaction between the hardener and the resin.
8. After mold has cured, (1-2 hours), pull mold apart.

Appendix B

List of Products and Suppliers

1. Pig Hearts
   Baringer Bros.
   Richlandtown, PA
   (215) 536-4337

2. Estane Polyurethanes
   BFGoodrich
   Specialty Polymers and Chemicals Div.
   Cleveland, Ohio
   (800) 543-2912

3. Stepless Ear Clamps
   Oetiker, Inc.
   Livingston, NJ
   (201) 992-1920

4. General Suppliers
   C & H Sales Co.
   Pasadena, CA
   (800) 325-9465

5. McMaster-Carr Supply Co.
   New Brunswick, NJ
   (201) 329-3200

6. Silicone II Rubber Sealant
   General Electric Co.
   King of Prussia, PA
   (215) 337-4430
   (Also available in hardware stores)

7. Microcrystalline Wax
   Dick Blick's Art Supply
   Bethlehem, PA

8. Plastic casting resin, hardener, and flexible molding material
   Mac's Hobby Hall
   Bethlehem, PA

Appendix C

Important Contacts

Dr. Michael Sinclair - Cardiac Surgeon
Work (215) 821-8790
Home (215 395-8376

David Rice - Director of Microsurgery Laboratory
Lehigh Valley Hospital
(215) 776-8000

Vita

The author, son of Mr. and Mrs. John N. Pacella, was born in Pittsburgh, Pennsylvania on January 12, 1968. He graduated from Peters Township High School, located in McMurray, Pennsylvania, in 1986. He received a Bachelor of Science degree in Mechanical Engineering with a Biomedical Emphasis from Carnegie Mellon University in 1990. Several of his summers were spent working at Allegheny General Hospital as a research engineer. He began pursuit of a Master of Science degree in Mechanical Engineering from Lehigh University in September 1990 as a Teaching Assistant. Presently he is employed as a project engineer, developing a new cardiac assist device at Allegheny General Hospital.

END OF TITLE